Applied Thermal Engineering 273 (2025) 126559

Contents lists available at ScienceDirect

Applied Thermal Engineering

journal homepage: www.elsevier.com/locate/apthermeng

Research Paper

Electrified distillation – Optimized design of closed cycle heat pumps with refrigerant selection and flash-enhanced mechanical vapor recompression

Momme Adami [a], Jonas Schnurr [a,b], Mirko Skiborowski [a,b,*]

[a] Hamburg University of Technology, Institute of Process Systems Engineering, Am Schwarzenberg-Campus 4, 21073 Hamburg, Germany
[b] United Nations University Hub on Engineering to Face Climate Change at the Hamburg University of Technology, United Nations University Institute for Water, Environment and Health (UNU-INWEH), Hamburg, Germany

ARTICLE INFO

Keywords:
Heat pump
Distillation
Vapor recompression
Electrification
Heat integration
Optimization
Refrigerant

ABSTRACT

Improving the energy efficiency of distillation processes is crucial for reducing the high energy demand and environmental impact of the chemical industry. Compression heat pumps play a significant role in this transformation as they are able to upgrade and recover heat rejected at low temperatures, reducing the need for external heat sources and simultaneously enable process electrification. Mechanical vapor recompression is the most prominent heat pump concept in distillation but limited by its reliance on process streams, which can lead to high external heat demand, or even inapplicability of the concept due to thermal instability or mechanical compressor limitations. Closed cycle heat pumps are less explored, since they require an extra heat exchanger and increased temperature lift compared to mechanical vapor recompression. However, they can overcome some of the limitations by allowing for unrestricted selection of the most attractive refrigerant, which may outplay the structural disadvantages. The current study presents a novel design approach for rapid heat pump evaluation, applicable to any subcritical refrigerant solely based on temperature levels and duties. A two-step approach enables the identification of the best-performing refrigerant from a set of suitable candidates for a given distillation process, considering practical constraints such as the need for superheating to avoid condensation, as well as limits for the compressor discharge temperature and compression ratios. The most promising refrigerant and heat pump configuration is further evaluated by a techno-economical optimization based on a superstructure model for which the performance is compared with a novel mechanical vapor recompression design utilizing a vapor recycle and internal preheating. The optimization results not only showcase fully electrified distillation for all heat pump-assisted processes but also highlight that closed cycle heat pumps with proper refrigerant selection can provide significant energy and cost savings while clarifying the respective advantages and limitations of competing concepts.

1. Introduction

Greenhouse gas emissions are a major driver of climate change, leading to an increased risk of extreme weather events such as severe storms, catastrophic floods, and deadly heatwaves [1, p. 2]. To mitigate these effects, the Climate Protection Scenario 95 aims to reduce such emissions by 95 % compared to the 1990 levels [2]. Given the large impact of the chemical and refining industry, significant energy and thus emission reduction can be achieved by improving the energy efficiency of especially separation processes [3]. As of today, distillation processes, which account for 90–95 % of all fluid separations [4, pp. 4–13], are the largest contributors to the respective energy demand of this industry. Yet, distillation processes are not easily replaced, by alternative technologies like membrane processes, due to their ability to handle a wide range of throughputs and producing high-purity products over a wide range of feed concentrations [5]. As highlighted in recent work by Agrawal et al. [6–8], distillation is also not generally inefficient and can for various cases be more efficient than alternative membrane separations.

Conventional distillation utilizes high temperature heat at the reboiler while rejecting a similar amount of heat at a lower temperature at the condenser, such that they can be considered as heat engine that transforms the heat duty of the reboiler into separation work at the temperature of the condenser [9]. While many distillation columns are still utilizing cooling water or air for condensation, due to the low utility

* Corresponding author at: Hamburg University of Technology, Institute of Process Systems Engineering, Am Schwarzenberg-Campus 4, 21073 Hamburg, Germany.
E-mail address: mirko.skiborowski@tuhh.de (M. Skiborowski).

https://doi.org/10.1016/j.applthermaleng.2025.126559
Received 16 February 2025; Received in revised form 29 March 2025; Accepted 21 April 2025
Available online 22 April 2025
1359-4311/© 2025 The Author(s). Published by Elsevier Ltd. This is an open access article under the CC BY license (http://creativecommons.org/licenses/by/4.0/).

Nomenclature

b_F, b_R, b_K	binary decision variable of feed, reflux, boil-up
b_{K_Sum}, b_{R_Sum}	sum of b_K, sum of b_R
$\dot{B}$	molar bottom flow rate
BMC	Bare module capital cost
$c_{F,n}$	Continuous decision variable of stage n for the feed
c_P	specific heat capacity
$C_{0,Equip}$	historical capital cost of equipment
$C_{Cap,Base,Equip}$	base capital cost of any piece of equipment
$C_{Cap,total}$	total capital cost
$C_{Op,Ann}$	annual operating cost
$C_{Utility}$	price of utility
$\dot{D}$	molar distillate flow rate
e(z), $\partial e(z)/\partial z$	external equations, gradients of external equations
$\dot{F}$	molar feed flow rate
h_F	feed enthalpy
h_i	enthalpy at location i
h^L, h^V	specific liquid enthalpy, specific vapor enthalpy
Δh	enthalpy difference
$\Delta h_{i\rightarrow j}$	enthalpy difference between point i and j
i	interest rate
$\dot{K}$	molar boilup flow rate
$\dot{L}$	molar liquid flow rate
$\dot{n}$, $\dot{N}$	molar flow rate
n	stage number
n_{actual}	actual number of stages
n_{max}	maximum number of stages
M	penalty weighting factor
MF	module factor
MPF	material and pressure factor
obj	objective function
$p_{F,n}$, $p_{R,n}$, $p_{K,n}$	penalty terms for decision variable of feed, reflux, boil-up
p_{Dist}, p_{Bot}	pressure of distillate/bottom stream at the reboiler
p_{low}, p_{high}	low/high pressure level in heat pump cycle
$\dot{Q}$	transferred heat
$Q_{0,Equip}$	standard capacity of equipment
Q_{Equip}	actual capacity of equipment
$Q_{Utility}$	required amount of utility
R	universal gas constant
$\dot{R}$	molar reflux flow rate
t	depreciation period
t_a	annual operating time
T_C, T_H	low temperature level, high temperature level
T_i	temperature at point i
T^{Bot}_{Sat,V,p_Bot}	saturated vapor temperature of the bottom stream at the reboiler
T^{Dist}_{Sat,L,p_Dist}	saturated liquid temperature of the distillate at the condenser
T^{Ref}_i	temperature of the refrigerant at point i
T^{Ref}_{Sat,V,p_low}	saturated vapor temperature of the refrigerant at low pressure level
T^{Ref}_{Sat,L,p_high}	saturated liquid temperature of the refrigerant at high pressure level
ΔT	approach temperature
UF	inflation factor
$\dot{V}$	molar vapor flow rate
$\dot{W}$	required work
W_{el}	electrical compressor duty
x	mole fraction in liquid stream
y	mole fraction in vapor stream
$z_{F,i}$	mole fraction in feed stream of component i
γ	individual exponent for equipment
$\eta_{isentropic}$	isentropic efficiency
$\eta_{mechanical}$	mechanical efficiency
κ	isentropic exponent

cost, the low-value heat is wasted to the environment instead of being reused. As demonstrated in the work of Agrawal et al. [7,10] it is essential to use this heat either by proper integration with the remaining process or upgrading it by means of a heat pump to a level at which it can be utilized locally [11]. Besides heat integration, thermal coupling and multi-effect distillation, heat pumps are an important means for improving the sustainability of distillation processes [9]. Moreover, the implementation of heat pumps does not necessitate changes to the column shells or internals, making them a versatile solution not only for new systems but also to retrofit existing processes which allows for substantial energy savings in existing plants without the need for extensive modifications [12, p. 365]. Heat pumps also enable highly integrated designs in combination with one of the other energy integration methods, e.g. fully thermally coupled dividing wall columns with the waste heat recovered, upgraded and integrated with the reboiler, to achieve particularly low energy requirements [13].

Heat pumps offer the unique transformative opportunity for an electrification of industrial processes and electrifying distillation in particular. This can significantly enhance the sustainability, by substantially reducing the net energy requirement and simultaneously transform distillation to a net-zero emission technology, when making use of renewable electricity from sources such as wind turbines or photovoltaics [14].

A variety of heat pump systems can be used to upgrade available heat [12]. However, compression heat pumps are the major type of heat pumps, which are applied in a variety of applications, residential as well as industrial heating, ventilation, air conditioning, and drying [5]. Compression heat pumps are described by a left-handed circular process that requires driving forces for the heat flows. Energy is transferred in the form of work and/or heat during a change of state. Different driving forces can be used to create the pressure changes between different temperature levels. The two main two driving forces are mechanically and thermally driven compression, of which mechanical compression is most common and easiest to implement [12]. Alternatives include absorption heat pumps, hybrid heat pumps and thermo-acoustic heat pumps [5].

The implementation of heat pumps in industry is currently still limited due to several reasons. Few manufacturers offer heat pump equipment capable of providing high temperatures required for industrial applications [15]. Furthermore, the industry lacks knowledge about the use of high-temperature heat pumps, which often necessitate the design of costly, specialized systems [16]. Moreover, heat pumps generally require a large investment, likely resulting in longer payback periods despite potentially large savings in operating costs compared to conventional heating [16]. The investment cost is largely driven by the cost of the compressor, which depends on the compressor work and volumetric flow rate. In vacuum systems, the volumetric flow rate is high due to the low vapor density, requiring larger diameter piping and compressors to handle the high volume flow [17].

In addition to these economic challenges, there are technical limitations to the application of compressors, especially for demanding industrial applications. At high discharge temperatures, the lubricating oil can decompose and contaminate the working fluid and even some working fluids may break down at very high temperatures [12]. Woods [18, p. 46] gives a maximum discharge temperature of 120–150 °C as a rule of thumb similar to the practical limit of 130–150 °C reported by

Kiss and Ferreira [12], who also specify temperatures up to 200 °C as feasible for vapor recompression (VRC). Generally, post-compression temperatures beyond ~150 °C are considered technically challenging but heat sink temperatures of up to 165 °C have been reported by Arpagaus *et al.* [16] with modified commercial equipment. Another limitation depending in the compressor type is the compression ratio, which is typically around 2–4 for centrifugal compressors, with a practical limit of ~8 for most types of compressors, even though some reciprocating compressors are capable of compression ratios as high as 12 at low flow rates [12,18,19]. Recently, centrifugal compressors with compression ratios of 10–12 have also been presented [20–22]. High compression ratios can be mitigated by operating multiple compressors in series at identical compression ratios in the form of multistage compression or using multiple cascaded heat pumps with individual working fluid cycles and potentially different refrigerants, which however require further increased investment cost [12,19]. Similar to the discharge temperature, the economic limit is usually reached before the technical limit [12, p. 216].

Cyclic heat pump processes in the two-phase region of the state diagram can be described by the ideal left-hand Clausius-Rankine processes shown in Fig. 1, of which the first step is an isentropic pressure increase ($1 \rightarrow 2'$) of the vapor phase, followed by the isobaric reversible energy exchange in the form of heat with the condensation of the working fluid ($2' \rightarrow 3$). The condensed working fluid is expanded during the isentropic pressure reduction ($3 \rightarrow 4'$) and finally, heat is exchanged reversibly during the isobaric evaporation of the working fluid ($4' \rightarrow 1$).

For real processes, entropy increases irreversibly during the compression ($1 \rightarrow 2$) and relaxation ($3 \rightarrow 4$), resulting in a higher temperature at point (2) than after the isentropic pressure increase to point ($2'$) due to the course of the isobars in the vapor phase. The isentropic efficiency

$$\eta_{isentropic} = \frac{h_{2'} - h_1}{h_2 - h_1} \tag{1}$$

describes this irreversibility as the enthalpy difference of the isentropic pressure increase ($h_{2'} - h_1$) and the enthalpy difference of the real pressure increase ($h_2 - h_1$).

The operating principle of compression heat pumps is based on the relationship between the boiling temperature of a fluid and its pressure. The temperature difference between the condensation temperature (3) and evaporation temperature (1) of the refrigerant is known as the 'temperature lift'. The compressor duty and, consequently, the performance of heat pumps depend on the temperature lift, as higher temperature lifts require larger compression ratios. A larger compression ratio results in increased energy demand of the compressor, leading to higher investment and operational costs [12, p. 4]. The coefficient of performance (COP)

$$COP_{Heating} = \frac{\left|\dot{Q}_{Heating}\right|}{\dot{W}} = \frac{\dot{Q}_{Cooling} + \dot{W}}{\dot{W}} = COP_{Cooling} + 1 \tag{2}$$

is commonly used to evaluate the performance of different heat pump systems based on the transferred heat $\dot{Q}$ and required work $\dot{W}$. The COP of a heat pump is always smaller than the theoretical COP of an ideal Carnot process

$$COP_{Carnot} = \frac{T_H}{T_H - T_C} \tag{3}$$

which only depends on the low (T_C) and high (T_H) temperature levels assuming that the cycle is fully reversible. Consequently, the COP values are higher in case of small temperature lifts and thus less work is required for applying heat pumps to distillation columns which separate close boiling systems [23]. This is an extremely important aspect for heat-pump assisted distillation, since classical heuristics rather focus the use of distillation towards systems with a sufficient relative volatility, which require less separation effort in terms of the number of equilibrium trays and reflux ratio, but considers wide boiling systems as preferential use cases for distillation [24,25]. While the separation by means of distillation is more challenging for close boiling systems, the possible COP of heat-pump assisted distillation is larger in comparison to wide boiling systems.

In order to evaluate this trade-off and provide a thorough comparison between mechanical vapor recompression and closed-cycle heat pumps, the current work presents a novel two-stage approach for the selection of suitable refrigerants and an optimization-based design for the evaluation of techno-economically optimized process configurations. The performance is compared to conventional distillation and VRC-assisted distillation with flash recycle and integrated preheater for additional heat integration. Before getting into detail on the proposed method, Section 2 presents a short summary on the different concepts for heat-pump assisted distillation, with specific focus on the use of external (closed cycle) heat pumps and refrigerants. Section 3 presents the details on the proposed two-stage approach, which is further illustrated in Section 4 for two case studies, representing a narrow boiling and a wide boiling mixture. The major conclusions are presented in Section 5, pointing out further objectives and needs for the identification of the most suitable heat-pump assisted distillation process.

2. Heat pump assisted distillation

There are a number of different operating principles for heat pump assisted distillation systems, with varying working fluids and operating cycle, considering open cycle heat pumps in VRC and bottom flashing (BF), closed cycle external heat pumps (EHP), as well as the concept of internally heat integrated distillation columns (HIDiC) [26]. The current work focusses on VRC and EHP, as both concepts can be implemented

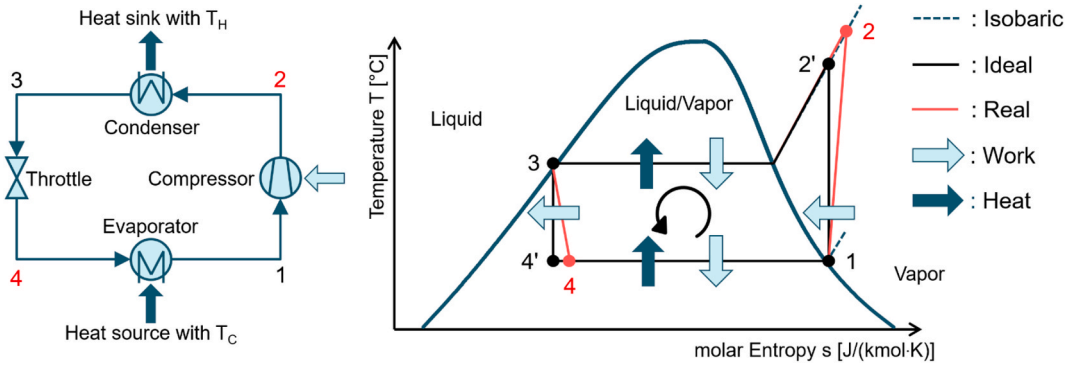

Fig. 1. Temperature-entropy diagram of heat pump (left) with idealand real Clausius-Rankine cycles (right).

for existing distillation columns without the need to modify the distillation column itself. While the heat pump itself is operated at lower pressures in BF potentially enabling safer operation than VRC [27], the setup usually requires operation of the distillation column at increased pressure [28]. BF is also considered to be more expensive than VRC, due to the lower pressure at the compressor and larger piping and equipment [29]. For HIDiC the whole distillation column is conceptually different, operating the stripping and rectifying section at different pressures, such that heat can directly be transferred from the rectifying to the stripping section [29,30]. While the idea of a diabatic column with continuous heat transfer is very intriguing, several studies have shown the potential benefits over VRC to be limited and oftentimes not sufficient for the increased complexity [31–33].

2.1. Vapor recompression

In mechanical VRC, the saturated vapor exiting the column serves as the working fluid and is compressed (1 → 2) in an open Clausius-Rankine cycle as displayed in Fig. 2 (left). An additional heat exchanger may be required upfront of the compressor to superheat the vapor in order to ensure a dry compression. The compression ratio is selected such that the boiling temperature of the compressed vapor is higher than the boiling temperature of the bottom product and some minimum approach temperature to provide (most of) the reboiler duty by condensation of the compressed vapor during heat integration in the reboiler (2 → 3). If the heat of condensation is insufficient to generate the required boil-up vapor, an additional steam-driven heat exchanger is added to provide the additional heat duty. After condensation, the working fluid is expanded (3 → 4), condensed to saturated liquid conditions (4 → 5) and split into reflux and distillate stream.

Mechanical VRC is the simplest heat pump concept in distillation and offers the advantage of requiring only a single approach temperature, because evaporation and condensation take place in a single heat exchanger, enabling savings of up to 80 % of the energy cost compared to conventional distillation [29]. As for all mechanical heat pump concepts, the energy savings are associated with a higher investment cost due to the compressor [34]. Interestingly, larger savings are possible for close boiling mixtures as these require smaller temperature lifts and accordingly lower compression ratios. For the separation of wide boiling mixtures, integration with an intermediate side reboiler with VRC can be a promising option [17]. This does not only enable a lower temperature lift, but can also reduce internal exergy losses inside the distillation column [8]. While the current contribution does not consider intermediate heat exchangers, we refer to the recent article of Skiborowski and Kruber [35] for a method to identify promising process structures with intermediate heat exchangers based on an analysis of the exergy requirements.

Despite its advantages, the practical application of VRC is often limited by several constraints related to the working fluid, its flow rate and heat pump design, which depend directly on the properties of the process medium. If the heat released during condensation of the top vapor, determined by its heat of vaporization at the high pressure level, is insufficient to meet the heat demand of the reboiler, this can result in potentially large amounts of unintegrated heat in addition to the external energy required for preheating.

To overcome this limitation, the traditional VRC-assisted distillation flowsheet can be modified to incorporate a flash recycle. The concept of flash vapor circulation was originally introduced by Modla and Lang [36] and later extended with a cooler after the throttling valve for pressure-swing distillation applications [37,38]. After the working fluid is (partially) condensed for heat integration with the reboiler, the resulting two-phase stream is split into vapor and liquid at the low pressure level and the vapor phase is recycled back to the compression cycle to increase the flow rate of the working fluid through the compressor. This approach minimizes the heat loss to cooling water and results in more available heat at the high-temperature level, thereby enhancing the efficiency of the system and improving the COP of the heat pump. Before entering the compressor, the combined working fluid stream can be preheated using an integrated heat exchanger as shown in Fig. 2 (right), further improving energy efficiency and facilitates full electrification of the process as only the compressor required externally supplied energy in the form of electricity. Other than the work of Cui *et al.* [39], who demonstrate this concept for methanol dehydration, and Nogaja *et al.* [40] who illustrate a further extended concept with additional cogeneration by means of simulation studies, the current work proposes and applies a superstructure optimization of such a flash-enhanced VRC design.

While such a VRC-assisted distillation process theoretically enables full electrification, additional challenges may limit practical implementation. If the top product exhibits strong superheating during compression due to steep isobaric curves in the vapor phase, as seen with substances like water or methanol, the temperature after compression may quickly exceed practical limits, rendering VRC with single-stage compression inapplicable. While multi-stage compression with intercooling (see e.g. [39]) or operation under vacuum conditions can be applied in such cases, such solutions often prove impractical due to additional cost for larger and more expensive piping and equipment. Moreover, beyond these thermodynamic constraints, it is crucial that the top product is suitable as a working fluid for compression and can be safely used at high temperatures. VRC becomes impractical in many cases where the process medium is prone to polymerization, thermal degradation, or contains corrosive or fouling components [12, p. 12].

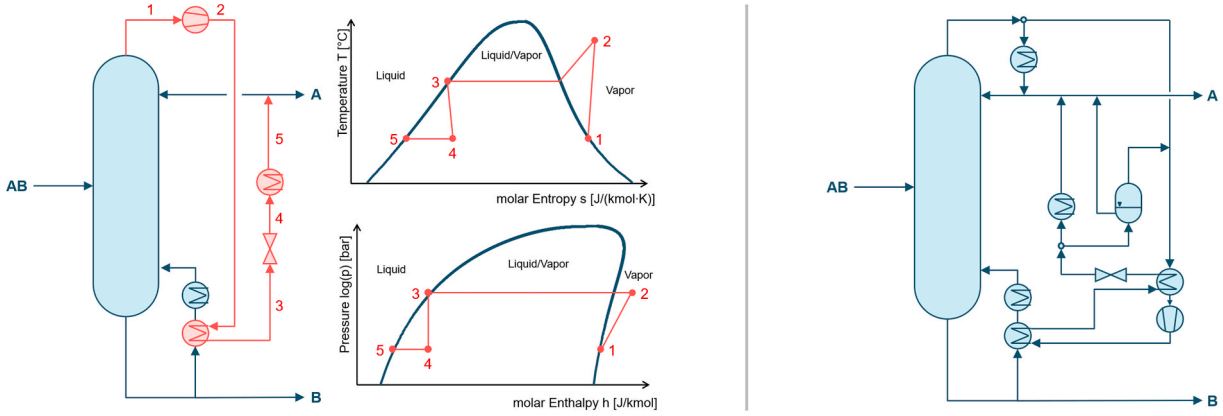

Fig. 2. Flowsheet of distillation column with traditional VRC (left) with corresponding T–s diagram and log(p)–h diagram of the distillate, and flowsheet with flash-enhanced VRC (right).

2.2. External heat pumps

In an external heat pump as shown in Fig. 3, a separate refrigerant that does not participate in the separation is used in a closed, externally located compression cycle, identical to the Clausius-Rankine cycle. Similar to VRC, additional heat exchangers may be required to provide additional duties if the top product is not fully condensed after heat exchange with the working fluid and if the heat provided by the heat pump is insufficient to fully vaporize the boil-up stream.

The main advantage of EHPs is that the working fluid can be chosen freely, so its properties and flow rate are entirely independent of separation process in contrast to VRC or bottom flashing. Not only does this allow the refrigerant flow rate to be freely selected for maximum heat integration, but it also allows the tailored selection of a substance with the best properties, to meet the specific requirements [17]. A substance already present in the process or any alternative can be selected as the working fluid, so EHPs can be applied in a wide range of conditions where other heat pump types are inapplicable [12, p. 12].

The COP of EHPs can be enhanced by increasing the heat uptake from the heat source by subcooling (4 → 5) the working fluid at the higher pressure level before expansion, leading to a greater difference in enthalpy during evaporation (6 → 1) [12, p. 206] as illustrated in the log (p)-h diagram in Fig. 4. As for the other heat pump concepts, the vapor needs to be superheated before entering the compressor for working fluids with a hanging two-phase envelope to ensure dry compression, as it would otherwise form liquid droplets during compression, which can cause damage to the compressor. If superheating is necessary, an additional heat exchanger and heat source are required. The additional heat exchanger can be implemented in the form of an internal heat exchanger (IHX) as shown in Fig. 4, eliminating the need for external heating and subcooling and resulting in an increased COP at the cost of more complex behaviour during start-up and limited operational flexibility for different temperature levels [41].

While closed-cycle heat pumps do of course require a larger temperature lift due to the secondary heat exchanger, this makes EHPs a simple retrofit option for existing distillation columns, since the actual process medium and column operation is entirely unaffected [29]. However, a leak in a heat exchanger may contaminate the product streams with refrigerant, whereas in other heat pump designs this only affects the composition of the product streams.

2.3. Refrigerants and selection criteria

The performance of EHPs is highly dependent on the refrigerant selected due to its thermal properties, which affect the compression cycle and required duty. The selection of a refrigerant for a process depends on a wide range of criteria, including thermal suitability, environmental friendliness, safety, energy efficiency and availability at reasonable cost [16].

A refrigerant is thermally suitable if its thermal properties match the temperature and pressure ranges of the process. The refrigerant should have a freezing temperature well below the evaporation temperature at the operating pressures [42, p. 2] and the critical temperature of the refrigerant should be well above the condensation temperature at the higher pressure level to avoid trans- or supercritical operation. At the evaporation temperature, the vapor pressure should be greater than 1 atm to avoid vacuum operation of the heat pump, as vacuum operation has potential performance and safety problems, if air enters the cycle.

A refrigerant is environmentally friendly if it complies with regulations restricting the use of certain refrigerants with the aim of eliminating the use of substances that deplete the ozone layer or have a high global warming potential (GWP) as refrigerants. The Ozone Depletion Potential (ODP) is a measure to determine the damage of this chemical to the ozone layer and indicates the relative amount of ozone depletion compared to R–11 (trichlorofluoromethane) with an ODP of one. If another refrigerant has an ODP of one, it will deplete as much as R-11, and an ODP of zero means that the refrigerant does not damage the ozone layer [42, p. 116]. The GWP is defined as the equivalent contribution of 1 kg carbon dioxide to the greenhouse effect over 100 years. A GWP of 100 means that 1 kg of this refrigerant has the same effect as 100 kg of carbon dioxide over a period of 100 years. When selecting a refrigerant for a process, the refrigerant must have an ODP of zero and a low GWP.

Additionally, refrigerants should be non-toxic, non-flammable and non-corrosive [19, p. 534]. Flammability and toxicity are indicated by a combination of a letter and a number from one to three in accordance with DIN EN 378-1 and ASHREA standards [43,44]. The letter A indicates a refrigerant with a lower toxicity and the letter B a refrigerant with higher toxicity. The number 1 represents a non-flammable refrigerant and number 3 marks a refrigerant with higher flammability [42, p. 115]. The auto-ignition temperature should also be at least 75 °C higher than the discharge temperature to avoid auto-ignition [41] and refrigerants should have a satisfactory solubility in the lubricating oil inside the compressor and this mixture should be thermally stable [16].

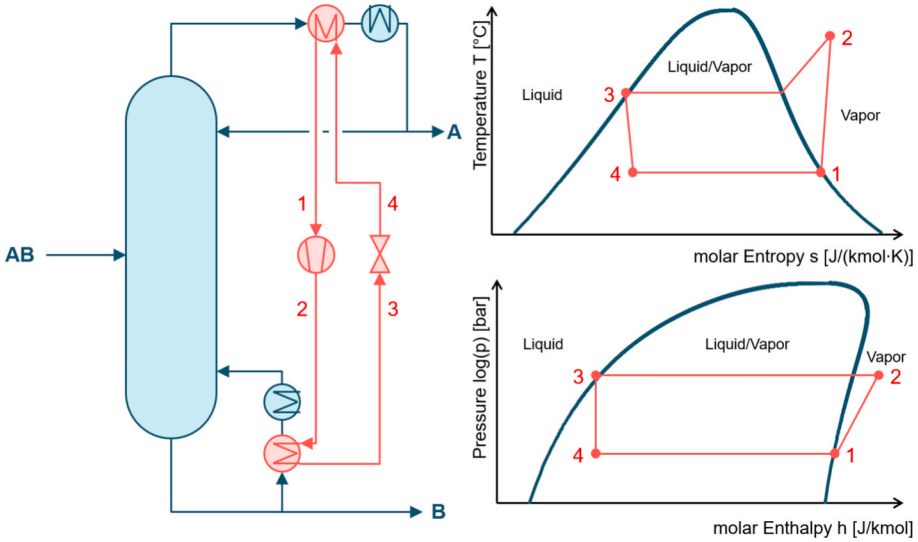

Fig. 3. Flowsheet of a distillation column with a closed cycle heat pump (left), T–s diagram (upper right) and log(p)–h diagram (lower right) of the refrigerant.

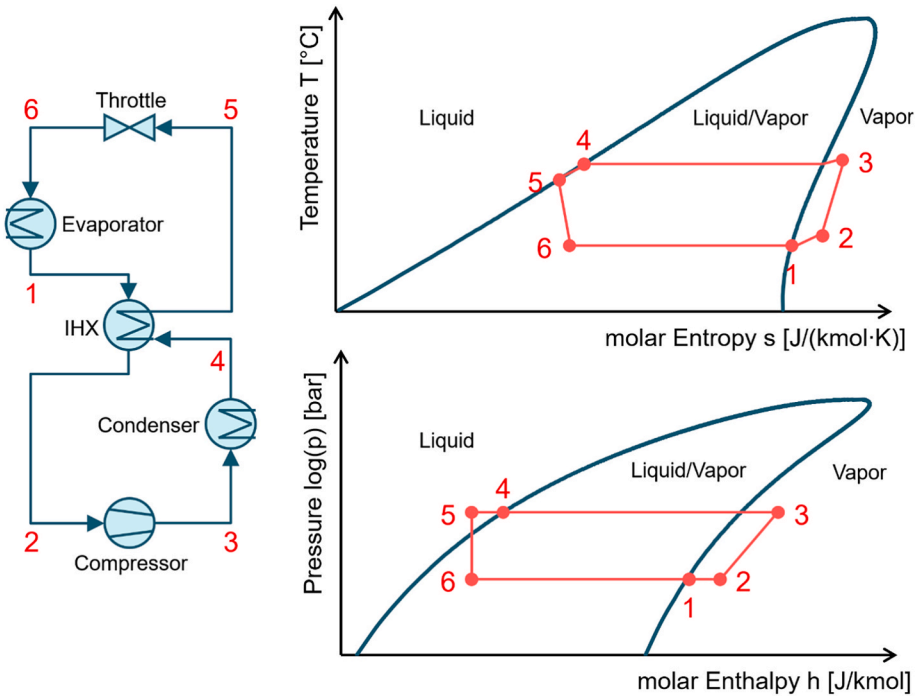

Fig. 4. Flowsheet (left), T-s diagram (upper right) and log(p)-h diagram (lower right) of a heat pump with internal heat exchanger.

The energy efficiency of a refrigerant for a process depends on the shape of the two-phase envelope. The critical pressure should be low, resulting in lower compression ratios [16] while the refrigerant should also have a large heat of vaporization for low refrigerant flow rates, reducing the power requirement. The latent heat decreases as the temperature increases and the critical point is approached. If the refrigerant has a wide range between normal boiling point and critical point, the performance of the process can be improved because the latent heat decreases slowly [45]. In addition, the fluid should have a relatively high vapor density to ensure that the volume flows and corresponding compressor size are small [28]. If the slope of the saturated vapor line in the temperature-entropy diagram is steep, the degree of superheating decreases, increasing the COP and reducing the required heat transfer area [19, p. 533].

The price and availability should be considered as the last criterion to decide between refrigerants that are performing equally in the other criteria, since a less expensive refrigerant may require more compressor work, ultimately resulting in higher cost. Since there is no universally optimal refrigerant that perfectly fits all criteria, a trade-off must be made between different refrigerants, depending on the specific use case and process conditions. There are several types of molecules that can be used as refrigerants with different strengths and weaknesses and the four specific classes of molecules considered in the scope of the current study are summarized in Table 1.

Chlorofluorocarbons (CFCs) and hydrochlorofluorocarbons (HCFCs) are partially or fully halogenated hydrocarbons composed of hydrogen, carbon, chlorine and fluorine, and have proven their efficiency as classic refrigerants by meeting most of the selection criteria [16,17]. However, CFCs and HCFCs have an ODP greater than zero and are prohibited for use in modern heat pump or cooling processes. The first attempt to replace these types of refrigerants was with hydrofluorocarbons (HFCs) which have an ODP of zero and are also thermally stable for most processes, but have a relatively high GWP and some HFCs are flammable. Therefore, these refrigerants are phased out [46]; alternatives should have an ODP of zero, a GWP of less than 150, low toxicity and marginal flammability [45].

Hydrocarbons (HCs) are natural working fluids with low GWP and ODP and are common substances in chemical plants but they are highly flammable [17,46]. Non-flammable natural molecules such as carbon dioxide, ammonia and water are possible refrigerants in addition to HCs. Carbon dioxide can be used for a transcritical process. The high latent heat of water makes it an attractive refrigerant for temperatures above 150 °C but it has a low vapor density, resulting in high volumetric flow rates [16] and it exhibits strong superheating during compression. Natural refrigerants have a good availability at low cost, limited toxicity, low environmental impact and good miscibility with each other. The increased flammability of some natural refrigerants is accepted because it is assumed that technically and economically feasible and safe solutions exist [47].

Hydrofluoroolefins (HFOs) are unsaturated organic compounds containing hydrogen, fluorine and carbon. HFOs are environmentally friendly alternatives to HFCs because they share many of the positive thermodynamic properties of CFCs. The double bond in these molecules makes them more readily degradable in the atmosphere, resulting in a low GWP [17]. Hydrochlorofluoroolefins (HCFOs) have similar properties to the HFOs, but have an ODP greater than zero, which could lead to restrictions on HCFOs in the future [16]. Another type of molecule that can be used as a refrigerant is hydrofluoroethers (HFEs) which contain an ether linkage, resulting in a shorter atmospheric lifetime and leading to a lower GWP than HFCs. HFEs have potential as a substitute for CFCs due to their comparable physical and thermophysical properties [48].

Despite the importance of the specific refrigerants for heat-pump assisted distillation with EHP, the scope of existing studies has so far been rather limited. The use of EHPs for distillation was first addressed by Supranto at al. [28,49] in in a series of publications in the 1980 s, which mostly focuses on experimental work with single refrigerants. Oliveira *et al.* [50] presented simulation studies for a simplified heat pump considering four refrigerants without further comparison with VRC. On the contrary such comparison was pursued by Reddy *et al.* [51], but using water as sole refrigerant, for which the use in heat pumps is limited by the high temperatures after compression. Recently, Rix *et al.* [17] presented a simulation-based comparison of EHPs considering eight different refrigerants and a comparison with VRC, specifically focusing on vacuum applications. They conclude that both VRC and EHP configurations can be used for a wide range of operating pressures and

Table 1
List of refrigerants (CP = critical pressure, CT = critical temperature, SG = safety group classification, BT = normal boiling temperature and Hvap = heat of vaporization at T = 70 °C).

Type	Name	R-Number	CP [bar]	CT [°C]	GWP	ODP	SG	BT [°C]	Hvap [kJ/kmol]
CFC	Trichlorofluoromethane	R-11	44.08	198.05	4750[a]	1[1)]	A1	23.82	22315.7
CFC	1,2-Dichloro-1,1,2,2-tetrafluoroethane	R-114	32.6	145.7	10040[1)]	1[1)]	A1	3.77	18373.6
HCFC	Dichlorofluoromethane	R-21	51.84	178.43	151[1)]	0.04[1)]	B1	8.9	20688.9
HCFC	3,3-Dichloro-1,1,2,3,3-pentafluoropropane	R-225ca	31.59	207.85	122[1)]	0.02[1)]	A1	50.1	25908.8
HFC	1,1,1,2-Tetrafluoroethane	R-134a	40.56	101.03	1430[1)]	0[1)]	A1	−26.07	12689.4
HFC	1,1-Difluoroethane	R-152a	45.198	113.29	124[1)]	0[1)]	A2	−24.02	13950.5
HFC	Ethyl-Fluoride	R-161	50.28	102.16	86[2)]	0[2)]	A3	−37.7	11511.2
HFC	1,1,1,3,3-Pentafluoropropane	R-245fa	36.4	154.05	1030[1)]	0[1)]	B1	15.3	21689.1
HFC	2,3-Dihydroperfluoropentane	HFC-4310mee	22.88	181.05	1700[3)]	0[3)]	A1	53.7	29145
HFO	Trifluoroethylene	R-1123	45.385	58.58	0.3[4)]	0[4)]	A2L	−61.395	–
HFO	1,1-Difluoroethylene	R-1132a	44.6	29.65	0.05[5)]	0[5)]	A2	−85.65	–
HFO	2,3,3,3-Tetrafluoropropene	R-1234yf	33.82	94.7	<1[6)]	0[6)]	A2L	−29	10987.7
HFO	1,3,3,3-Tetrafluoropropene	R-1234ze	36.62	109.36	<1[6)]	0[6)]	A2L	−18.32	14123.2
HFO	Cis-1,1,1,4,4,4-Hexafluoro-2-butene	R-1336mzz(Z)	28.9904	171.321	2[6)]	0[6)]	A1	33.422	23929.8
HCO	Trans-1,2-Dichloroethylene	R-1130	55.1	243.35	5[5)]	0.00024[5)]	B2	47.7	26875.9
HCFO	1-Chloro-3,3,3-trifluoropropene	R-1233zd	35.709	165.6	1[6)]	0.00034[6)]	A1	18.32	21504
HC	Methane	R-50	45.99	−82.586	25[7)]	0[7)]	A3	−161.49	–
HC	Ethane	R-170	48.72	32.17	6[7)]	0[7)]	A3	−88.6	–
HC	Propane	R-290	42.48	96.68	3[6)]	0[6)]	A3	−42.04	10081.1
HC	n-Butane	R-600	37.96	151.97	4[6)]	0[6)]	A3	−0.5	17884.4
HC	Isobutane	R-600a	36.4	134.65	3[6)]	0[6)]	A3	−11.72	15669.5
HC	n-Pentane	R-601	33.7	196.55	5[6)]	0[6)]	A3	36.07	23667.8
HC	2-Methly-butane	R-601a	33.8	187.25	5[8)]	0[8)]	A3	27.844	22152.5
HC	Hexane	–	30.25	234.15	3[9)]	0[9)]	A3	68.73	28796.6
HC	Heptane	–	27.4	267.05	3[9)]	0[9)]	A3	98.43	33693.3
HC	Ethylene	R-1150	50.41	9.19	4[7)]	0[7)]	A3	−103.74	–
HC	Propylene	R-1270	46	91.7	2[6)]	0[6)]	A3	−47.7	9012.25
HC	Acetone	–	47	234.95	n.a.	n.a.	A3	56.13	28208.3
HC	Cyclobutene	–	66.71	193.85	n.a.	0[8)]	A3	2.54	19602.6
HC	Cyclopentane	–	45.1	238.55	11[10)]	0[10)]	A3	49.25	26179.4
Ether	Diethyl-ether	R-610	36.4	193.55	4[7)]	0[7)]	A3	34.43	24058.5
Ether	Dimethyl-ether	RE-170	53.7	126.95	1[6)]	0[6)]	A3	−24.84	14723.2
Natural	Ammonia	R-717	112.8	132.5	0[6)]	0[6)]	B2L	–33.43	15996.7
Natural	Water	R-718	220.64	373.946	0[6)]	0[6)]	A1	100	42030.2
Natural	Carbon-Dioxide	R-744	73.83	31.06	1[9)]	0[9)]	A1	−78.45	–
Natural	Methanol	–	80.84	239.35	n.a.	n.a.	A3	64.7	34930.4
HFE	Ethyl-nonafluorobutyl-ether	HFE-7200	19.75	208.87	55[3)]	0[3)]	A1	76	31133.2
HFE	Difluoromethyl-2,2,2-trifluoroethylether	R-245mf	34.2	170.88	286[1)]	0[1)]	A1	29	24264
Fluoroketone	Dodecafluoro-2-methylpentan-3-one	Novec649	18.45	441.81	1[11)]	0[11)]	A1[11)]	49.05	25292.6

CP, CT, BT and Hvap values are provided by AspenPlus. Safety group classification based on DIN EN 378 and ASHRAE Standard 34 [43,44]. GWP and ODP values are taken from literature. If no value is available, n.a. is selected for not available.
1) : Daniel *et al.* [57],
2) : Fernández-Moreno *et al.* [41],
3) : 3 M Electronics Materials Division [58],
4) : Oh *et al.* [45],
5) : Giménez-Prades *et al.* [59],
6) : Arpagaus *et al.* [16],
7) : European parliament and of the council of the European Union [60],
8) : Höges *et al.* [61],
9) : SNAP [62],
10) : Gil and Kasperski [63],
11) : 3 M Deutschland [64].

temperature lifts, and have the potential to decrease energy and costs. They further highlight that EHP can offer better economic performance than VRC given the selection of a suitable working fluid for the specific application.

Some methods either focus primarily on the thermodynamic properties and safety aspects of a selection of different refrigerants, such as the work of like Mateu-Royo *et al.* [52] and Koundinya and Seshadri [53], who evaluate several selected refrigerants based on various energy, exergy, environmental, and economic criteria. Other authors proposed more general heuristics for the selection and assessment of heat pumps and refrigerants, such as Kiss *et al.* [23] and Jiang et al. [54]. The most general and recent methods pursue wide-ranged sensitivity studies for refrigerants and heat pump configurations [55] or the optimization of a hypothetical molecule and subsequent screening of a suitable refrigerant based on continuous molecular targeting [56], focusing on the COP and volumetric heating capacity. These methods focus however solely on the heat pump and have not yet been connected to applications in distillation.

3. Methods

In order to overcome the reliance on simplified heuristics or thermodynamic criteria for the evaluation of a handful of refrigerants a two-stage method is proposed. The first stage performs an automatic evaluation of a pool of potential refrigerants based on an initial shortcut computation for the distillation column for which a generalized model-based design approach for closed cycle heat pumps evaluates a large pool of 39 potential pure subcritical refrigerants. The evaluation builds on the temperature levels and heat duties of the distillation process provided from a thermodynamically-sound shortcut computation, and modifies the design of the heat pump cycle if required, to consider superheating before compression, counteracting possible condensation.

After identifying the most promising refrigerants under consideration of additional practical limitations, a techno-economic optimization of the process, considering the distillation columns and EHPs is performed. The performance of the resulting heat pump assisted distillation columns is further compared with optimized conventional and VRC-assisted distillation columns to analyze the techno-economic performance.

3.1. Shortcut model of distillation column with external heat pump

In order to evaluate the source and sink conditions for the application of the heat pump the minimum energy requirements and temperature levels of the condenser and reboiler are first determined for a specified separation task by means of the thermodynamically sound Rectification Body Method (RBM) [65]. The RBM does not rely on assumptions of constant relative volatilities or constant molar overflow and therefore can be applied for non-ideal and azeotropic mixtures. The geometrical pinch-based shortcut method assumes an infinite number of equilibrium stages and calculates the thermodynamic minimum energy demand for sharp splits without limitations on the number of components. The RBM can be interpreted as an extended version of the geometrical interpretation of the Underwood method. The reader is referred to the original work of Bausa *et al.* [65] for further details, as well as the overview of Skiborowski *et al.* [66] on pinch-based shortcut methods for distillation.

Based on the results of the shortcut computations, providing heat duties and temperature levels for heat sources and sinks assuming isobaric operation, the following calculations for the heat pump are performed, using on the flowsheet and state diagrams in Fig. 4. These computations are not limited for applications with distillation columns and provide a general model for closed cycle heat pumps with any possible refrigerant, provided the property parameters of the refrigerant and temperature level of the heat source and heat sink are known.

For the application as EHP in distillation, the lower pressure level p_{low} inside the heat pump is first selected such that the saturated vapor temperature of the refrigerant $T^{Ref}_{sat,V,p_{low}}$ is lower than the saturated liquid temperature of the distillate at the condenser $T^{Dist}_{sat,L,p_{Dist}}$ by a prespecified approach temperature ΔT.

$$T^{Ref}_{sat,V,p_{low}} = T^{Dist}_{sat,L,p_{Dist}} - \Delta T \tag{4}$$

The pressure after compression p_{high} is then determined using flash calculations and chosen such that the saturated liquid temperature of the refrigerant $T^{Ref}_{sat,L,p_{high}}$ is greater than the saturated vapor temperature of the bottom stream at the reboiler $T^{Bot}_{sat,V,p_{Bot}}$ by the specified approach temperature.

$$T^{Ref}_{sat,L,p_{high}} = T^{Bot}_{sat,V,p_{Bot}} + \Delta T \tag{5}$$

If this pressure exceeds the critical pressure of the refrigerant, the refrigerant is considered thermodynamically unsuitable, as it would result in a trans- or supercritical heat pump process and the calculation is terminated for this particular refrigerant.

If the temperature after isentropic compression is lower than the saturated vapor temperature of the refrigerant at the higher pressure, superheating prior to compression is necessary to avoid condensation during compression due to a hanging two-phase envelope as shown in Fig. 4. An IHX provides the superheating duty by subcooling the refrigerant ($\Delta h_{4\to5}$) after the condensation at the higher pressure. In this case, the specific enthalpy of the refrigerant

$$h_5\left(T^{Ref}_5, p_{high}\right) = h_4\left(T^{Ref}_{sat,L,p_{high}}, p_{high}\right) - \left(h_2\left(T^{Ref}_2, p_{low}\right) - h_1\left(T^{Ref}_{sat,V,p_{low}}, p_{low}\right)\right) \tag{6}$$

leaving the IHX at the higher pressure is calculated, based on the specific enthalpy after evaporation which is determined based on the saturated vapor temperature of the refrigerant at the lower pressure level ($h_1\left(T^{Ref}_{sat,V,p_{low}}, p_{low}\right)$). The specific enthalpy after condensation is the saturated liquid enthalpy at the higher pressure ($h_4\left(T^{Ref}_{sat,L,p_{high}}, p_{high}\right)$), while the conditions at the compressor inlet with a temperature greater than the saturated vapor temperature of the refrigerant by the degree of superheating result in $h_2\left(T^{Ref}_2, p_{low}\right)$. The temperature after superheating T^{Ref}_2 is selected as the lowest temperature such that no condensation occurs during isentropic compression.

After calculation of the specific enthalpy h_3 following the polytropic compression from state (2 → 3) using the isentropic efficiency based on (1)

$$h_3\left(T^{Ref}_3, p_{high}\right) = h_2\left(T^{Ref}_2, p_{low}\right) + \frac{h_{3'}\left(T^{Ref}_{3'}, p_{high}\right) - h_2\left(T^{Ref}_2, p_{low}\right)}{\eta_{isentropic}}, \tag{7}$$

the refrigerant flow rate

$$\dot{n}_{Refrigerant,Reboiler} = \frac{\dot{Q}_{Reboiler,original}}{|\Delta h_{3\to4}|} = \frac{\dot{Q}_{Reboiler,original}}{\left|h_4\left(T^{Ref}_{sat,L,p_{high}}, p_{high}\right) - h_3\left(T^{Ref}_3, p_{high}\right)\right|} \tag{8}$$

for full integration of the original reboiler duty $\dot{Q}_{Reboiler,original}$ and refrigerant flow rate

$$\dot{n}_{Refrigerant,Condenser} = \frac{\left|\dot{Q}_{Condenser,original}\right|}{\Delta h_{6\to1}} = \frac{\left|\dot{Q}_{Condenser,original}\right|}{h_1\left(T^{Ref}_{sat,V,p_{low}}, p_{low}\right) - h_6\left(T^{Ref}_6, p_{low}\right)} \tag{9}$$

for full integration of the original condenser duty $\dot{Q}_{Condenser,original}$ are calculated with an isenthalpic throttle ($h_5\left(T^{Ref}_5, p_{high}\right) = h_6\left(T^{Ref}_6, p_{low}\right)$). The smaller of the two flow rates is utilized as the flow rate of the working fluid $\dot{n}_{Refrigerant}$ in order to fully integrate the smaller of evaporation and condensation duty. If no IHX is needed, the enthalpy of the working fluid at the compressor inlet is equal to the enthalpy of the saturated vapor at the lower pressure ($h_1\left(T^{Ref}_{sat,V,p_{low}}, p_{low}\right) = h_2\left(T^{Ref}_2, p_{low}\right)$ and the enthalpy of the saturated liquid at the higher level is equal to the enthalpy before the throttle ($h_4\left(T^{Ref}_{sat,L,p_{high}}, p_{high}\right) = h_5\left(T^{Ref}_5, p_{high}\right)$).

In case of any excess heat duties, additional heat exchangers ensure liquid product and reflux streams, depending on how the refrigerant flow rate was selected. If the molar flow rate required to fully integrate the condenser duty is used, a remaining reboiler duty

$$\dot{Q}_{Reboiler} = \dot{Q}_{Reboiler,original} - \dot{n}_{Refrigerant} \cdot \left|h_4\left(T^{Ref}_{sat,L,p_{high}}, p_{high}\right) - h_3\left(T^{Ref}_3, p_{high}\right)\right| \tag{10}$$

needs to be provided as the original reboiler duty $\dot{Q}_{Reboiler,\,original}$ cannot be integrated. Alternatively, if the molar flow rate required to fully integrate the reboiler duty is used, a remaining condenser duty

$$\dot{Q}_{Condenser} = \dot{Q}_{Condenser,original} + \dot{n}_{Refrigerant} \cdot \left|h_1\left(T^{Ref}_{sat,V,p_{low}}, p_{low}\right) - h_6\left(T^{Ref}_6, p_{low}\right)\right| \tag{11}$$

is required as the original condenser duty $\dot{Q}_{Condenser,\,original}$ cannot be integrated. Both condenser duties are defined as negative values. Finally, the electrical compressor duty

$$\dot{W}_{el} = \dot{n}_{Refrigerant} \cdot \Delta h_{2\to3} = \dot{n}_{Refrigerant} \cdot \frac{h_3\left(T^{Ref}_3, p_{high}\right) - h_2\left(T^{Ref}_2, p_{low}\right)}{\eta_{mechanical}} \tag{12}$$

is calculated with the mechanical efficiency $\eta_{mechanical}$.

3.2. Rigorous optimization-based design

A rigorous techno-economic optimization is performed on the basis of equilibrium stage superstructure model based on the MESH equations posed in the General Algebraic Modeling System (GAMS), a high-level algebraic modeling language with access to automatic differentiation tools and state-of-the-art solvers. The next subsections provide an overview of three distinct models for a conventional distillation column and columns integrated with flash-enhanced VRC or EHP and the respective solution procedures. All models for the calculation of the distillation column assume an isobaric operation and the separation task is defined by constraints for the product purities. The individual optimization problems are solved as a series of successively-relaxed mixed-integer nonlinear programming (MINLP) problems with a polylithic initialization and solution strategy.

3.2.1. Superstructure model for conventional distillation columns

The superstructure model of a conventional column, as shown in Fig. 5, enables a variable size for the rectifying and stripping section, by allowing the reflux and boil-up streams to be distribute to variable stages in the superstructure. Additionally, the feed stream may be distributed along the height of the column, which adds excess flexibility to the superstructure. A detailed description of the superstructure models and the solution procedure of conventional columns can be found in Kraemer *et al.* [67] and Skiborowski *et al.* [68]. The remainder of the section provides a short summary of the main model equations.

Each equilibrium tray in the superstructure model is described by the MESH equations, which include mass balances, equilibrium calculations, summation constraints and enthalpy balances. The mass balance of a general stage n is defined as:

$$\dot{L}_{n-1}\cdot x_{n-1,i} + \dot{V}_{n+1}\cdot y_{n+1,i} + \dot{F}\cdot z_{F,i}\cdot b_{F,n} + \dot{R}_n\cdot x_{1,i}\cdot b_{R,n} + \dot{K}_n\cdot y_{n_{max},i}\cdot b_{K,n} = \dot{L}_n\cdot x_{n,i} + \dot{V}_n\cdot y_{n,i}, \quad n \in [2,\ n_{max}-1] \tag{13}$$

with $\dot{L}_n$ and $\dot{V}_n$ being the flow rates and $x_{n,i}$, $y_{n,i}$ the composition of component i for the liquid and vapor phases leaving stage n. $\dot{F}$, $\dot{R}_n$, $\dot{K}_n$, $z_{F,i}$, $x_{1,i}$ $y_{n_{max},i}$ are the flow rate and the composition of the feed, reflux and boil-up streams. The superstructure allows variable locations for the feed, reflux and boil-up locations to define the effective number of stages for both sections. These decisions are reflected by binary decision variables $b_{F,n}$, $b_{R,n}$ and $b_{K,n}$, which determine if the feed, reflux or boil-up is directed to stage n. Depending on the reflux and boil-up decision variables, some stages at the top of the column have no liquid flow and some stages at the bottom of the column have no vapor flow, rendering them ineffective to the separation. These stages are consequently considered non-existing in the final evaluation of the column height. The sum of each decision variable across all stages is set to 1 to fulfill the mass balance:

$$\sum_n b_{R,n} = 1, \quad \sum_n b_{K,n} = 1, \quad \sum_n b_{F,n} = 1. \tag{14}$$

The according enthalpy balance is defined as

$$\dot{L}_{n-1}\cdot h^L_{n-1} + \dot{V}_{n+1}\cdot h^V_{n+1} + \dot{F}\cdot h_F\cdot b_{F,n} + \dot{R}_n\cdot h^L_1\cdot b_{R,n} + \dot{K}_n\cdot h^V_{n_{max}}\cdot b_{K,n} = \dot{L}_n\cdot h^L_n + V_n\cdot h^V_n, \quad n \in [2,\ n_{max}-1] \tag{15}$$

Considering specific liquid h^L_n and vapor enthalpies h^V_n, as well as the enthalpies of the feed h_F, reflux h^L_1 and boil-up $h^V_{n_{max}}$. As indicated in Fig. 6 the enthalpies as well as the vapor–liquid equilibrium computations are performed by means of external equations, considering rigorous thermodynamic models. We refer to Skiborowski *et al.* [68] for further details as well as Section 4 and the Supporting Information for the specific thermodynamic models considered in the current work. The mass and enthalpy balances of the condenser

$$\dot{V}_2\cdot y_{2,i} = \dot{D}\cdot x_{1,i} + \dot{R}\cdot x_{1,i}, \tag{16}$$

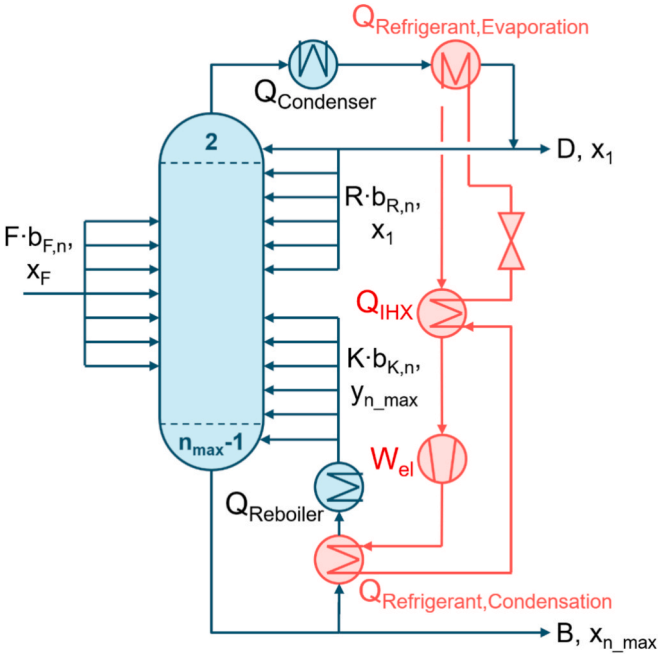

Fig. 6. Superstructure of distillation column with external heat pump cycle in red. (For interpretation of the references to colour in this figure legend, the reader is referred to the web version of this article.)

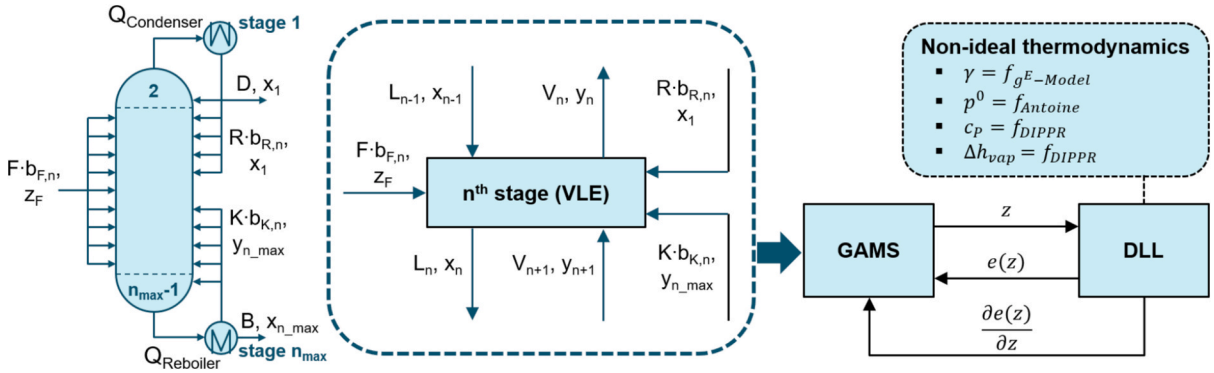

Fig. 5. Superstructure of simple distillation column and conjunction of GAMS with external function [69].

$$\dot{V}_2 \cdot h_2^V = \dot{D} \cdot h_1^L + \dot{R} \cdot h_1^L - \dot{Q}_{Condenser}, \tag{17}$$

with the total condenser duty $\dot{Q}_{Condenser}$ and the mass balance and enthalpy balances of the partial reboiler

$$\dot{L}_{n_{max}-1} \cdot x_{n_{max}-1,i} = \dot{B} \cdot x_{n_{max},i} + \dot{K} \cdot y_{n_{max},i}, \tag{18}$$

$$\dot{L}_{n_{max}-1} \cdot h^L_{n_{max}-1} + \dot{Q}_{Reboiler} = \dot{B} \cdot h^L_{n_{max}} + \dot{K} \cdot h^V_{n_{max}}, \tag{19}$$

with duty $\dot{Q}_{Reboiler}$ are defined similarly, with enthalpy and equilibrium computations performed as external equations. The model furthermore considers the overall mass balance

$$\dot{F} = \dot{D} + \dot{B}, \tag{20}$$

with $\dot{D}$ and $\dot{B}$ as distillate and bottom flow rate and the enthalpy balance

$$\dot{F} \cdot h_F + \dot{Q}_{Reboiler} = \dot{D} \cdot h_1^L + \dot{B} \cdot h^L_{n_{max}} - \dot{Q}_{Condenser}. \tag{21}$$

Summation equations are considered for all of the liquid and vapor mole fractions:

$$\sum_i x_{n,i} = 1, \quad \sum_i y_{n,i} = 1. \tag{22}$$

The external equations are introduced in the form of a dynamic link library (DLL) as shown in Fig. 5, whereas in each iteration of the optimization, a set of variables z is transferred from GAMS to the external function which returns the results of the evaluation of the external equations $e(z)$ and the gradients of the external equations $\frac{\partial e(z)}{\partial z}$. This can be considered as a reduced space formulation of the optimization problem, which limits the number of variables and equations handled by GAMS [68].

3.2.2. Modification of optimization model for external heat pump

For the implementation of the EHP based on the flowsheet shown in Fig. 6, only the energy balances at the reboiler and condenser stages of the superstructure model of the conventional column need to be modified.

The overall energy balance around the entire column including the EHP with electrical compressor duty $\dot{W}_{el}$ is modified to

$$\dot{F} \cdot h_F + \dot{Q}_{Reboiler} + \dot{W}_{el} = \dot{D} \cdot h_1^L + \dot{B} \cdot h^L_{n_{max}} - \dot{Q}_{Condenser}. \tag{23}$$

$\dot{Q}_{Condenser}$ and $\dot{Q}_{Reboiler}$ are provisional to provide remaining external duties after heat integration to ensure saturated liquid conditions for the reflux and distillate. The energy balance of the condenser

$$\dot{V}_{n+1} \cdot h^V_{n+1} = \dot{D} \cdot h_1^L + \dot{R} \cdot h_1^L - \dot{Q}_{Condenser} + \dot{Q}_{Refrigerant,Evaporation}, \tag{24}$$

includes the term $\dot{Q}_{Refrigerant,Evaporation}$ that specifies the heat required for the evaporation of the refrigerant in the heat integrated condenser. The energy balance of the reboiler

$$\dot{Q}_{Reboiler} + \dot{L}_{n_{max}-1} \cdot h^L_{n_{max}-1} - \dot{Q}_{Refrigerant,Condensation} = \dot{B} \cdot h^L_{n_{max}} + \dot{K} \cdot h^V_{n_{max}}, \tag{25}$$

includes $\dot{Q}_{Refrigerant,Condensation}$ as the heat released during condensation of the refrigerant in the heat integrated reboiler. The energy balance only around the heat pump

$$\dot{W}_{el} + \dot{Q}_{Refrigerant,Evaporation} = -\dot{Q}_{Refrigerant,Condensation} \tag{26}$$

links these two via the electrical compressor duty

$$\dot{W}_{el} = \dot{n}_{WF} \cdot \frac{h_{Compressor,Out} - h_{Compressor,In}}{\eta_{mechanical}} \tag{27}$$

which is calculated with the enthalpy difference of the compression multiplied by the molar flow rate $\dot{n}_{WF}$ of the working fluid. The duties of the heat integrated reboiler and the heat integrated condenser are calculated similarly as the product of the enthalpy difference of the respective heat exchanger and the refrigerant flow rate as

$$\dot{Q}_{Refrigerant,Evaporation} = \dot{n}_{WF} \cdot \left(h_{Refrigerant,Evaporation,Out} - h_{IHX,Out}\right), \tag{28}$$

$$\dot{Q}_{Refrigerant,Condensation} = \dot{n}_{WF} \cdot \left(h_{Refrigerant,Condensation,Out} - h_{Compressor,Out}\right). \tag{29}$$

If an IHX is required to provide superheating, its enthalpy balance is defined as

$$h_{IHX,Out} - h_{Refrigerant,Condensation,Out} = -\left(h_{Compressor,In} - h_{Refrigerant,Evaporation,Out}\right), \tag{30}$$

and is used to indirectly determine the amount of heat transferred

$$\dot{Q}_{IHX} = \dot{n}_{WF} \cdot \left(h_{IHX,Out} - h_{Refrigerant,Condensation,Out}\right) \tag{31}$$

If the IHX is not actually required $\dot{Q}_{IHX} = 0$.

All enthalpies are calculated with the previously introduced external equations based on the temperature and pressure levels. In order to maintain the same type of external equations, which evaluate saturated liquid and vapor conditions, additional pressure and temperature variables are introduced for non-saturated conditions as shown in Fig. 7 (left). The additional variables are controlled using equality constraints.

The compression is modeled in a simplified way by the isentropic relation for an ideal gas following the approach introduced by Harwardt and Marquardt [32]. The isentropic output temperature

$$T_{Compressor,isentropic,out} = T_{Compressor,in} \cdot \left(\frac{p_{high}}{p_{low}}\right)^{\frac{\kappa-1}{\kappa}} \tag{32}$$

is calculated as a function of the input temperature $T_{Compressor,in}$, the compression ratio $\frac{p_{high}}{p_{low}}$ and the isentropic exponent

$$\kappa = \frac{c_p}{c_p - R} \tag{33}$$

which depends on the universal gas constant R and the specific heat capacity c_p. The isentropic efficiency

$$\eta_{isentropic} = \frac{\Delta h_{isentropic}}{\Delta h} = \frac{c_p \cdot (T_{Compressor,isentropic,out} - T_{Compressor,in})}{c_p \cdot (T_{Compressor,out} - T_{Compressor,in})} \tag{34}$$

is used to calculate the output temperature of a polytropic compression. A combination of Eq. (29) and Eq. (34) gives the equality constraint used to model the compression

$$T_{Compressor,out} = T_{Compressor,in} \cdot \left(1 + \frac{1}{\eta_{isentropic}} \left(\left(\frac{p_{high}}{p_{low}}\right)^{\frac{\kappa-1}{\kappa}} - 1\right)\right) \tag{35}$$

Dry compression is ensured by an inequality constraint

$$T_{Compressor,isentropic,out} \geq T_{sat} \tag{36}$$

on the temperature after compression in relation to the temperature T_{sat} of the saturated vapor of the working fluid at increased pressure, which is again computed by an external equation.

3.2.3. Modification of optimization model for flash-enhanced vapor recompression

The VRC model shown in Fig. 8 is based on the work of Waltermann and Skiborowski [69] and implemented similarly to the EHP model. The differences lie in the specific energy balances and compression cycle which is extended with several constraints modeling an internal heat exchanger and the option to recycle low pressure vapor to allow for larger working fluid flow rates for additional heat integration.

The overall energy balance reads as

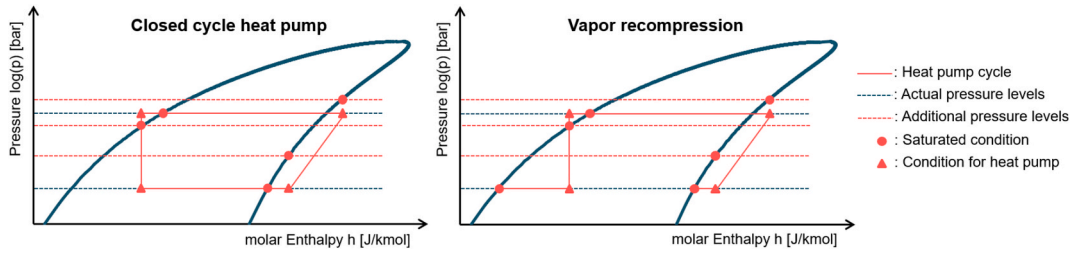

Fig. 7. Log(p)-h diagram of a closed cycle heat pump and VRC with additional pressure levels.

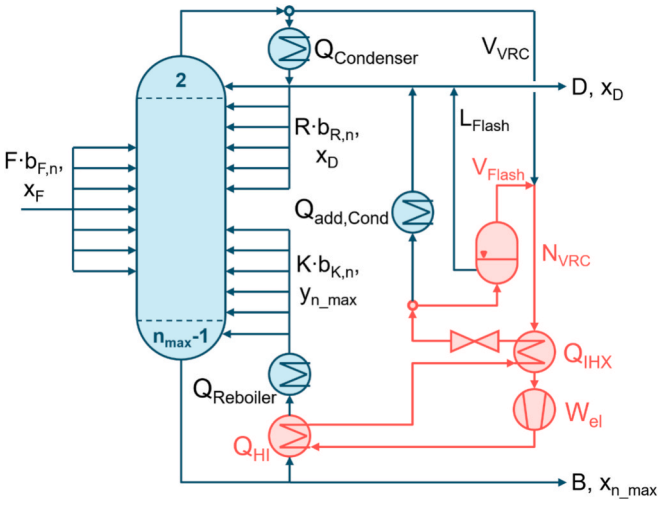

Fig. 8. Superstructure of distillation column with flash-enhanced vapor recompression. The compression cycle is highlighted in red. (For interpretation of the references to colour in this figure legend, the reader is referred to the web version of this article.)

$$\dot{Q}_{Reboiler} + \dot{W}_{el} + \dot{F}\cdot h_F = \dot{D}\cdot h^L_{n_1} + \dot{B}\cdot h^L_{n_{max}} - \dot{Q}_{Condenser} - \dot{Q}_{add,Cond}, \tag{37}$$

the reboiler energy balance as

$$\dot{Q}_{Reboiler} + \dot{Q}_{HI} = \dot{L}_{n_{max}-1}\cdot h^L_{n_{max}-1} + \dot{B}\cdot h^L_{n_{max}} + \dot{K}\cdot h^V_{n_{max}} \tag{38}$$

including the additional heat duty $\dot{Q}_{Reboiler}$ and the work $\dot{W}_{el}$ for VRC. The respective energy balance for the heat pump is

$$\dot{W}_{el} + \dot{V}_{n+1}\cdot h^V_{n+1} = \dot{D}\cdot h^L_D + \dot{R}\cdot h^L_D - \dot{Q}_{HI} - \dot{Q}_{Condenser} - \dot{Q}_{add,Cond}, \tag{39}$$

and the electrical compressor duty is calculated according to Eq. (27). The additional pressure levels for the VRC model are presented in Fig. 7 (right). The calculations for the compression are similar to those presented in Eqs. (32)–(35) for closed cycle compression in Section 3.2.2, however the vapor leaving the top of the column with flow rate $\dot{V}_2$ can be split into a vapor serving as the working fluid and a part that is conventionally condensed $\dot{V}_{Condenser}$.

$$\dot{V}_2 = \dot{V}_{Condenser} + \dot{V}_{VRC} \tag{40}$$

$$\dot{Q}_{Condenser} = \dot{V}_{Condenser}\cdot\left(h^V_2 - h^L_1\right) \tag{41}$$

The vapor entering the compression cycle $\dot{V}_{VRC}$ is mixed adiabatically with the recycled vapor stream $\dot{V}_{Flash}$ that is separated in a flash vessel after expansion to the lower pressure level.

$$\dot{N}_{VRC} = \dot{V}_{VRC} + \dot{V}_{Flash} \tag{42}$$

$$\dot{N}_{VRC}\cdot z_{VRC,i} = \dot{V}_{VRC}\cdot y_{2,i} + \dot{V}_{Flash}\cdot y_{Flash,i} \tag{43}$$

$$\dot{N}_{VRC}\cdot h_{VRC} = \dot{V}_{VRC}\cdot h^V_2 + \dot{V}_{Flash}\cdot h^V_{Flash} \tag{44}$$

Dry compression is ensured by an inequality constraint similar to Eq. (36) which enforces that the temperature after compression is greater than or equal to the temperature of the saturated vapor at increased pressure. The amount of heat transferred in the internal heat exchanger is

$$\dot{Q}_{IHX} = \dot{N}_{VRC}\cdot\left(h^V_{Compressor,in} - h_{VRC}\right). \tag{45}$$

The stream after the expansion can be split into a stream $\dot{N}_{Flash}$ that is split into liquid and vapor phase in a flash vessel, with

$$\dot{N}_{VRC} = \dot{N}_{add,Cond} + \dot{N}_{Flash} \tag{46}$$

and a stream to an additional condenser $\dot{N}_{add,Cond}$ for full condensation to saturation conditions with

$$\dot{Q}_{add,Cond} = \dot{N}_{add,Cond}\cdot\left(h^L_{add,Cond} - h^L_{IHX}\right). \tag{47}$$

The flash vessel is described by the overall mass balance, component mass balance, enthalpy balance and summation equations.

$$\dot{N}_{Flash} = \dot{L}_{Flash} + \dot{V}_{Flash} \tag{48}$$

$$\dot{N}_{Flash}\cdot z_{VRC,Flash,i} = \dot{L}_{Flash}\cdot x_{Flash,i} + \dot{V}_{Flash}\cdot y_{Flash,i} \tag{49}$$

$$\dot{N}_{Flash}\cdot h^L_{IHX} = \dot{L}_{Flash}\cdot h^L_{Flash} + \dot{V}_{Flash}\cdot h^V_{Flash} \tag{50}$$

$$\sum x_{Flash} = \sum y_{Flash} = 1 \tag{51}$$

The heat released by the condensation of the compressed vapor during heat integration

$$\dot{Q}_{HI} = \dot{N}_{VRC}\cdot\left(h^L_{HI} - h^V_{Compressor,Out}\right) \tag{52}$$

are determined on the basis of the enthalpy h^l_{HI} of the saturated high-pressure liquid leaving the integrated reboiler. The specific enthalpies are calculated for the respective state variables (x,y,p,T) by means of the aforementioned external equations.

The reflux and distillate stream result from the individual shares that are summarized in the overall mass balance, component mass balance and enthalpy balance.

$$\dot{D} + \dot{R} = \dot{N}_{add,Cond} + \dot{L}_{Flash} + \dot{V}_{Cond} \tag{53}$$

$$\dot{D}\cdot x_{D,i} + \dot{R}\cdot x_{D,i} = \dot{N}_{add,Cond}\cdot z_{VRC,i} + \dot{L}_{Flash}\cdot x_{Flash,i} + \dot{V}_{Cond}\cdot y_{2,i} \tag{54}$$

$$\dot{D}\cdot h^L_D + \dot{R}\cdot h^L_D = \dot{N}_{add,Cond}\cdot h^L_{add,Cond} + \dot{L}_{Flash}\cdot h^L_{Flash} + \dot{V}_{Cond}\cdot h^L_1 \tag{55}$$

3.2.4. Equipment sizing and cost calculation

The calculation of capital cost builds on sizing and costing of the major pieces of equipment of the process, which are the column shell, tray stacks or packings (including liquid distributors, liquid collectors

and support grid) depending on the utilized type of internals, heat exchangers and compressors. The costs for the flash vessel are considered negligible as it does not need to hold large volumes and is at the same pressure as the column. Capital costs for the refrigerant are not considered, assuming that they are negligible in case there is no leakage. Even under conservative estimates (2,000 kg at 20 €/kg), the refrigerant cost (~40,000 €) amounts to only less than 4 % of the overall capital investment for the wide-boiling system in section 4.2.2 below, confirming that differences in refrigerant pricing are of minor significance in the overall process economics.

Equipment costs are calculated using Biegleŕs updated module factor method which extends Guthriés method with inflation correction factors and module factors to account for economies of scale [70, pp. 132–133]. The base capital cost

$$C_{Cap,Base,Equip} = C_{0,Equip} \cdot \left(\frac{Q_{Equip}}{Q_{0,Equip}} \right)^{\gamma} \tag{56}$$

of any piece of equipment is calculated with the historical cost $C_{0,Equip}$ and the standard capacity $Q_{0,Equip}$. An individual exponent γ is assigned to each piece of equipment, while Q_{Equip} refers to its actual capacity.

The capacity of heat exchangers is the required heat exchange area, which is calculated from the amount of heat exchanged and the logarithmic mean temperature difference, or the absolute temperature difference for heat exchangers that just exchange latent heat. For compressors, the capacity is equal to the compression duty. For column shell and tray stack, the column volume serves as the capacity and depends on the height and diameter, which is determined based on the vapor flow rate at the bottommost stage.

The actual number of stages in the column

$$n_{actual} = n_{max} - \sum_{n} b_{R_{Sum\,n}} - \sum_{n} b_{K_{Sum\,n}} + 2 \tag{57}$$

is calculated by subtracting all stages above the reflux tray and all stages below the boil-up tray from the maximum number of stages n_{max} [67]. The variable

$$b_{R_{Sum\,n}} = \sum_{j \geq n}^{n_{max}} b_{R,j} \tag{58}$$

is equal to 1 for all stages from the boil-up tray to the reboiler and the variable

$$b_{K_{Sum\,n}} = \sum_{j=1}^{j \leq n} b_{K,j} \tag{59}$$

for all stages from the condenser to the reflux tray. Therefore n_{actual} is corrected by (+2) to make-up for the boil-up and reflux tray.

The total capital cost $C_{Cap,total}$ is the sum of the bare module capital cost

$$BMC = UF \cdot C_{Cap,Base,Equip} \cdot (MF + MPF - 1) \tag{60}$$

for each piece of equipment, calculated based on the base capital cost, the inflation factor *UF*, the module factor *MF* and the material and pressure factor *MPF* [70, p. 135].

The inflation factor is equal to the present cost index divided by the base cost index, for which the Chemical Engineering Plant Cost Index (CEPCI) of 2024 is used. The module factor corrects for installation cost and economy of scale and depends on the base capital cost of the equipment. A combination of correction factors specific to the type of equipment determines the material and pressure factor with carbon steel used for all pieces of equipment. A more detailed overview of the design choices and correction factors based on Biegler [70] is given in the Supporting Material.

The annual operating cost

$$C_{Op,ann} = t_a \cdot \sum C_{Utility} \cdot Q_{Utility} \tag{61}$$

depends on the annual operating time t_a, which is assumed as 8000 h and the price $C_{Utility}$ and required amount $Q_{Utility}$ of each utility. The costs for the specific utilities derived from Turton [71, p. 231] are shown in Table 2.

The total annualized costs (*TAC*) represent the objective function for the process optimization and is calculated from a depreciated total capital cost and annual operating cost

$$TAC = \frac{i \cdot (1+i)^t}{(1+i)^t - 1} \cdot C_{Cap,total} + C_{Op,ann} \tag{62}$$

It depends on the annual payment for the capital cost and interest accrued over the lifetime of the process with interest rate i and depreciation period t in years. An interest rate of 6 % and a depreciation period of ten years are assumed in the current study.

3.2.5. Solution procedure

The resulting MINLP problems are solved as a series of successively relaxed NLP problems, following previously published polylithic modeling and solution strategies [67,68,72]. Accordingly, the problem is solved locally in a stepwise manner, with each subsequent step increasing the complexity of the problem while providing good initial values for the next step. The initialization and solution strategy presented in Fig. 9 is based on the approach of Skiborowski *et al.* [68].

The initialization and solution procedure begins with the 'fixed structure', which uses the maximum number of equilibrium stages by fixing the binary decision variables for the location of the feed, reflux and boil-up, resulting in an NLP. The first step of the initialization is a flash calculation of the feed at the column pressure to provide initial compositions and temperatures for each stage. Next, a conventional column with a fixed number of equilibrium stages is calculated by first solving the mass- equilibrium and summation (MES) equations before incorporation of the enthalpy balances (MESH). Afterwards, the optimal operating point of the column with a fixed structure is determined by minimizing the reboiler duty while considering the purity constraints.

While the initial steps are identical for the conventional column and models with heat pumps, the next steps differ based on the type of process. For a column with either of the heat pump types, the pressure levels of the working fluid are determined next so that the temperature differences in the heat exchangers are minimal. Afterwards, the energy balances and additional constraints for the respective heat pump are included and the results from the heat pump design calculated with the approach from Section 3.1 are used to specify the inlet temperature of the compressor for EHP. If superheating is required before compression, the inlet temperature is determined by

$$T_{Compressor,In} = T_{Refrigerant,Evaporation,Out} + \Delta T_{Superheating}. \tag{63}$$

If superheating is not required, the inlet temperature of the compressor is set equal to the dew point of the refrigerant at the low pressure level. After the extended model is solved, the isentropic exponent is updated to account for changing temperature and pressure levels before optimizing the operating conditions of the heat pump-assisted column. For EHP, the externally supplied energy is minimized. For VRC, initially the reboiler duty is minimized for a fixed equal stream splitting, after which the split is relaxed and the externally supplied energy is minimized. In the next

Table 2
Utilities and price of the utilities [71, p. 231].

Utility	Utility price [$/GJ]	Utility price [$/Common unity]
Cooling water (30 °C)	0.354	0.0148 €/t
Hot steam (6 bar, 160 °C)	14.05	29.29 €/t
Electricity	16.80	0.06 €/kWh

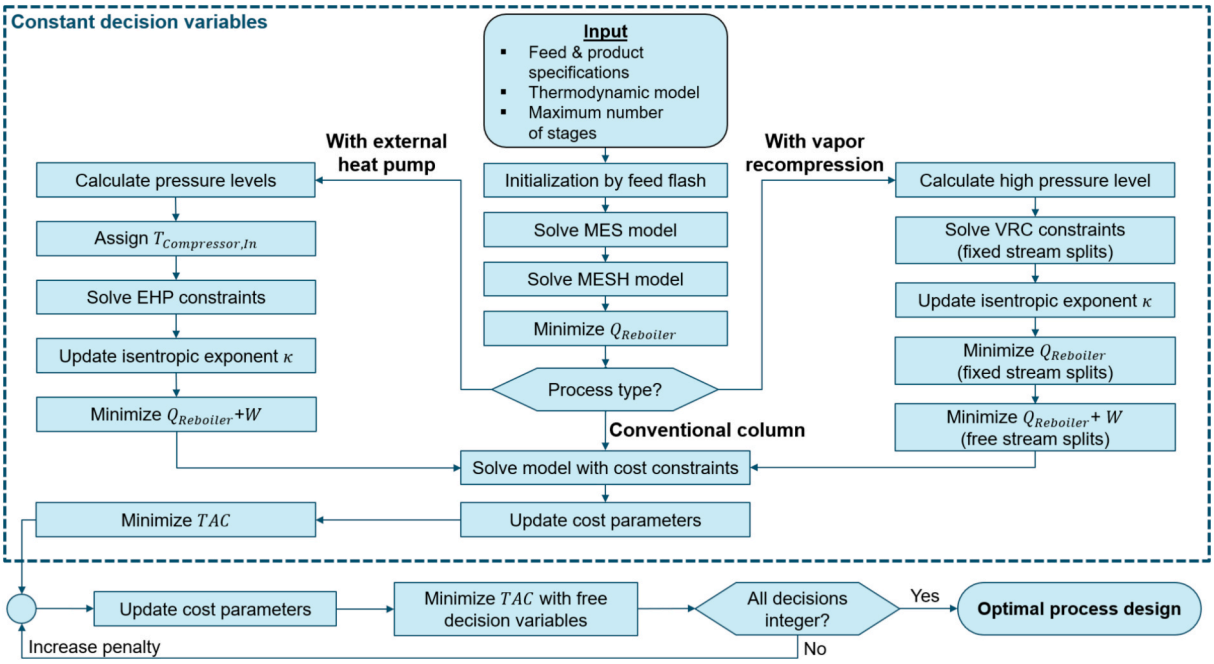

Fig. 9. Solution procedure for optimization a conventional column without and with EHP or VRC.

step, the all models are solved with added constraints for equipment sizing and costing (cf. Section 3.2.4). The last step in the fixed structure is the minimization of the TAC after updating the cost parameters to match the current design.

During all steps of the initialization (dashed blue box in Fig. 9), the maximum number of stages defined for the superstructure is enforced. In the final minimization of the TAC the feed, reflux, and boil-up locations are released in order to determine the most economic process design with variable number of stages in each column section. The solution of the respective MINLP problem is obtained by solving a series of successively relaxed NLP problems for which the binary decision variables are relaxed to continuous variables between 0 and 1, following the strategy by Kraemer *et al.* [67]. In order to derive integer solutions for these variables, additional nonlinear constraints in the form of Fischer-Burmeister functions are defined as penalty terms, shown here for the binary decision for the feed tray

$$p_{F,n} = c_{F,n} + \sum_{m \neq n} c_{F,m} - \sqrt{c_{F,n}^2 + \left(\sum_{m \neq n} c_{F,n}\right)^2}. \tag{64}$$

In this context, the continuous decision variable $c_{F,n}$ is introduced to represent the relaxed binary decision regarding the feed tray location. The penalty terms for reflux ($p_{R,n}$) and boil-up positions ($p_{K,n}$) are calculated identically and the sum of all penalties, multiplied by a weighting factor M, is added to the TAC in the modified objective function

$$obj_{modified} = TAC + M \cdot \left(\sum_n p_{F,n} + \sum_n p_{R,n} + \sum_n p_{K,n}\right). \tag{65}$$

Thus, non-discrete values of the decision variables are penalized. The penalty weighting factor is increased by a factor of 10 in a series of successive NLP optimizations, gradually increasing the impact of the penalty terms on the objective function. The iterations are aborted when all three decision variables are either 1 or 0 for each stage of the column.

4. Case studies

For the illustration of the method two case studies are examined, one for a close-boiling and one for a wide-boiling mixture, considering the separation of an equimolar saturated liquid feed at 10 mol/s into pure products. The close boiling mixture of benzene and fluorobenzene exhibits boiling points of 80.3 °C and 85.2 °C, with a difference of just 4.9 K, at atmospheric conditions, while hexanol and decanol have boiling points of 92.5 °C and 151.7 °C under vacuum conditions at 80 mbar, resulting in a temperature difference of 59.4 K. Considering an approach temperature of 10 K this requires working fluid condensation temperatures in the heat pumps of 95.2 °C for the close boiling system and 161.7 °C for the wide boiling system. While temperatures above ~150 °C pose particularly high demands on the compressor design as noted in Section 1, this situation is chosen here to illustrate the design and performance of heat pumps operating at the edge of current technical feasibility. For all studies, an isentropic efficiency of 85 % and a mechanical efficiency of 95 % is assumed, based on Rix *et al.* [17].

After screening all 39 refrigerants listed in Table 1 by means of the shortcut-based screening in terms of thermodynamically feasibility and their practical applicability, the best refrigerants are selected and a techno-economic optimization is performed, in order to provide a closer analysis of the performance of simple distillation columns and heat pump-assisted columns with VRC and EHP. All computations build on the extended Antoine equation in combination with the UNIQUAC model for the nonideality of the liquid and the Redlich-Kwong equation of state for the nonideality of the vapor phase, while DIPPR correlations are applied for the specific heat capacity and heat of vaporization. The respective property parameters are extracted from the Aspen Plus PURE39 and NIST-TRC database and provided in the form of text files. The utilized property parameters for the separated mixtures are listed in the Supporting Material.

4.1. Screening of refrigerants

All 39 candidates from Table 1 are first evaluated in respect of the required pressure inside the heat pump, considering them as thermodynamically unsuitable in case this pressure is higher than the critical pressure. Furthermore, as discussed in Section 1, refrigerants are considered practically unsuitable in case the compressor discharge temperature exceeds 180 °C and all pressure levels in the heat pump need to be above 1 atm to avoid vacuum processes. For the compression

ratio, common heuristics state values between 4–6 for single stage compression [73], while ratios beyond 10 have been reported for ultra-high pressure ratio centrifugal compressors [21]. In the current study an upper limit of 7 is selected for single stage compressors to avoid very costly compressor designs. Additional environmental and safety criteria for refrigerants like GWP, ODP, flammability or toxicity are not considered in this study in order to enable a performance analysis, but can easily be included to further narrow down the candidates prior to process optimization.

4.1.1. Refrigerant screening for separation of the close boiling mixture ($\Delta T = 4.9$ K)

Based on the initial feasibility criteria, 30 thermodynamically subcritical refrigerants are considered feasible and the respective minimum energy demand according to the shortcut-based screening is displayed in Fig. 10. For all refrigerants, regardless of the need for superheating, the entire heat is provided by the heat pump, so that only electricity is required for running the compressor and no external heat needs to be supplied. The EHP does consequently enable full electrification of the distillation column, significantly reducing the net energy demand by 78 % (R290) to 91 % (R1130) compared with a conventional column, which requires 2.69 MW of heat. The COPs for heating of the best performing refrigerants are at ~11, which is high for real world-applications, but much lower than the COP for the ideal Carnot process of 72.8.

The refrigerants R161, R134a and R290 all require comparatively high energy demands of 0.35 MW or higher resulting in COP values below 7.2, which results from operation very close (87 %, 89 % and 97 %) to their respective critical pressure. This leads to a low heat of vaporization near the critical point and thus high molar flow rate required to provide the heat for the separation.

The compression ratios of all thermodynamically suitable refrigerants lie between 1.58 (R290) and 2.71 (water = R718) which generally can be accomplished with a single stage centrifugal compressor [18,70]. However, while water (R718) is the third best refrigerant in terms of net energy demand, it would require sub-atmospheric operation of the heat pump as illustrated in Fig. 11. Therefore, it is excluded alongside heptane and HFE7200, due to vacuum operation.

The compressor discharge temperature of all refrigerants is close to 100 °C as shown in Fig. 12 except for water (R718, 181 °C), methanol (135 °C) and ammonia (R717, 125 °C) due strong superheating along steep isobaric curves in the T-s-diagram of these substances (see Supplementary Material Fig. S11-S13). Yet none of the discharge temperatures other than that of water exceeds the threshold value of 180 °C.

Based on the shortcut-based screening the top five refrigerants regarding net energy demand are selected from the remaining 27 practically feasible refrigerants and their performance data is summarized in Table 3. For this separation problem, R1130 is the best refrigerant in terms of total energy demand, but it is considered highly toxic and has an ODP above zero which likely poses problems in real-world application. Cyclopentane with a confirmed ODP of zero is the third best option in terms of net energy demand, but has the downside of being flammable and needing an additional heat exchanger for superheating. To avoid the need for an IHX, acetone may instead be used as it is also a hydrocarbon and thus likely has a low GWP and ODP of zero, which is however not confirmed to our knowledge. Since even R11, despite extremely high GWP and OPD, performs within 5.4 % of the energy demand of R1130, any of the top five refrigerants can be chosen without significant performance drawbacks. A decision based on such environmental or practical restrictions is also feasible, though not undertaken in this case. The T-s and log(p)-h diagrams of the top five refrigerants are shown in Section 4 of the Supporting Material.

4.1.2. Refrigerant screening for separation of the wide boiling mixture ($\Delta T = 59.4$ K)

The screening procedure is performed identically for the separation of the wide boiling mixture consisting of hexanol and decanol. Here, only 19 of the 39 refrigerants are thermodynamically feasible. The net energy demand for the respective heat pump-assisted distillations according to the shortcut calculations is shown in Fig. 13 (left). Again, only electricity for running the compressor is necessary, enabling full electrification for all refrigerants. However, the reduction of the net energy demand varies widely between 7 % (Novec649) and 73 % (R718 = water) compared to the conventional column, which requires 408.2 kW of heat. Consequently, the COP values are much lower compared to the close boiling system, with a COP for heating of 3.78 for the best performing refrigerant water at about 50 % of the COP of the Carnot process of 7.32. The energy demand of the worst performing refrigerants is again particularly high, as they operate close to the critical pressure, e.g. at 88 % of critical pressure for Novec649 and at 93 % for R1233zd.

While thermodynamically interesting, R718 (water) and methanol require impractically high discharge temperatures for a single stage compression beyond 250 °C (Fig. 13 (right)) and are consequently excluded from further consideration along with R21 with a discharge temperature of 185 °C. Fig. 14 (left) illustrates the strong superheating for water in the T-s diagram, which results in a significant excess in

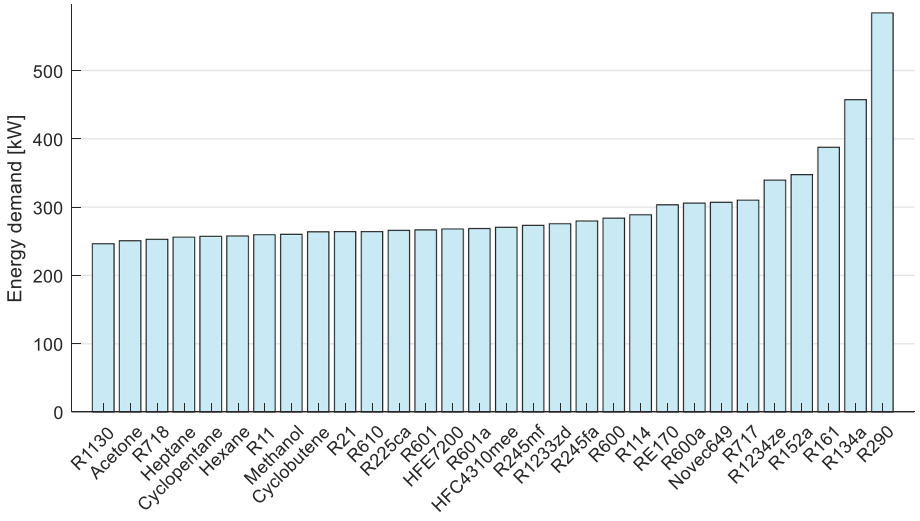

Fig. 10. Total energy demand of column with EHP for thermodynamically feasible refrigerants for separation of benzene-fluorobenzene.

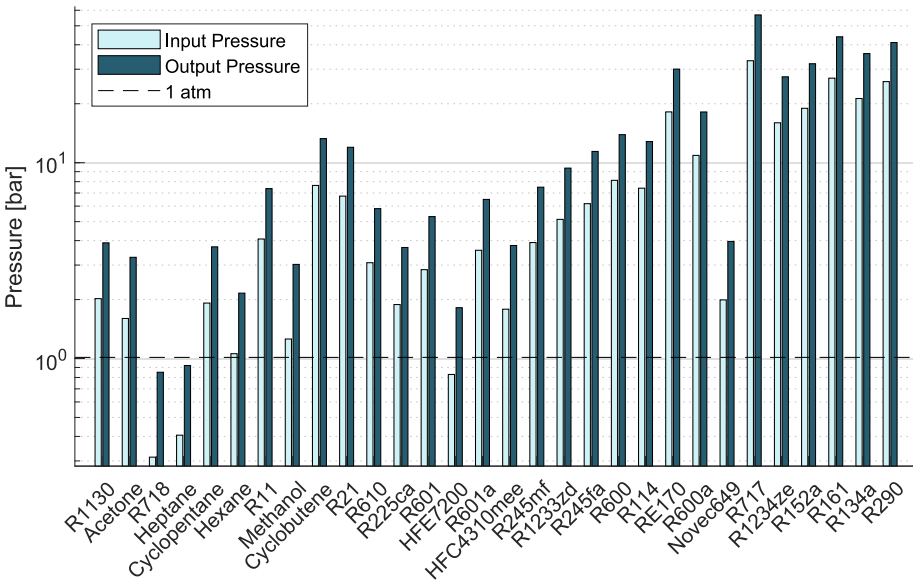

Fig. 11. Pressure levels of heat pumps for thermodynamically feasible refrigerants for separation of benzene-fluorobenzene.

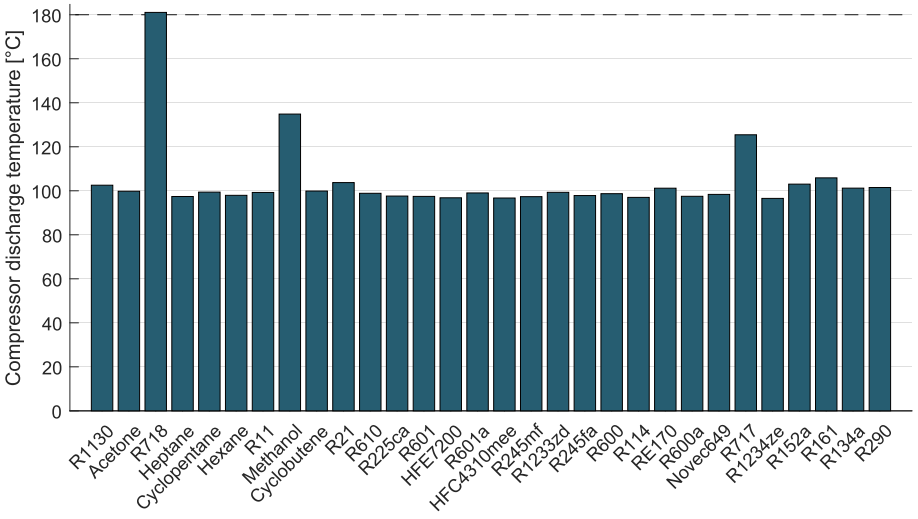

Fig. 12. Compressor discharge temperature of heat pumps for thermodynamically feasible refrigerants for separation of benzene-fluorobenzene.

Table 3
Top five refrigerants in terms of energy demand for separation of benzene-fluorobenzene.

Refrigerant	R1130	Acetone	Cyclopentane	Hexane	R11
Energy demand [kW]	246.3	250.9	257.2	257.7	259.7
$COP_{heating}$ [-]	11.36	11.16	10.88	10.86	10.78
Compression ratio [-]	1.93	2.05	1.94	2.04	1.81
Superheating duty [kW]	0	0	68.5	200.0	22.9
Logarithmic mean temperature difference in IHX [K]	–	–	20.1	14.7	23.4
Refrigerant flow rate [mol/s]	107.6	99.8	111.6	101.7	132.7

discharge temperature, compared e.g. to acetone, which is illustrated in Fig. 14 (right). In the following, all refrigerants with a discharge temperature below 180 °C are considered technically feasible in this study. This limit may be further reduced when operating the column at higher vacuum, e.g. reaching a discharge temperature of 150 °C for cyclopentane, if the column pressure is reduced to 35 mbar, but this again requires modifications of the operating conditions. The effects of different column pressures on the discharge temperatures, suitable refrigerants and resulting energy demand can easily be studied with the shortcut-based refrigerant screening and are presented in Section 5 of the Supporting Material.

While already discarded, it is also interesting to note that water and methanol also require the highest compression rations as shown in Fig. 15 (right). As expected, the compression ratios are generally much higher compared to the close boiling system and range from 4.19 for cyclobutene to 12.42 for water (R718). Based on the limiting compression ratio of 7, heptane and HFE7200 are excluded as well.

Notably, the same five refrigerants identified for the benzene-fluorobenzene separation are also identified as those requiring the lowest net energy demand and the performance metrics are listed in Table 4, indicating a more general suitability of these refrigerants for the temperature ranges considered for distillation in this study. Opposed to the close boiling system, acetone does however require superheating for the temperature levels of the hexanol-decanol separation, as displayed in the T-s diagram in Fig. 14 (right) with the operating points.

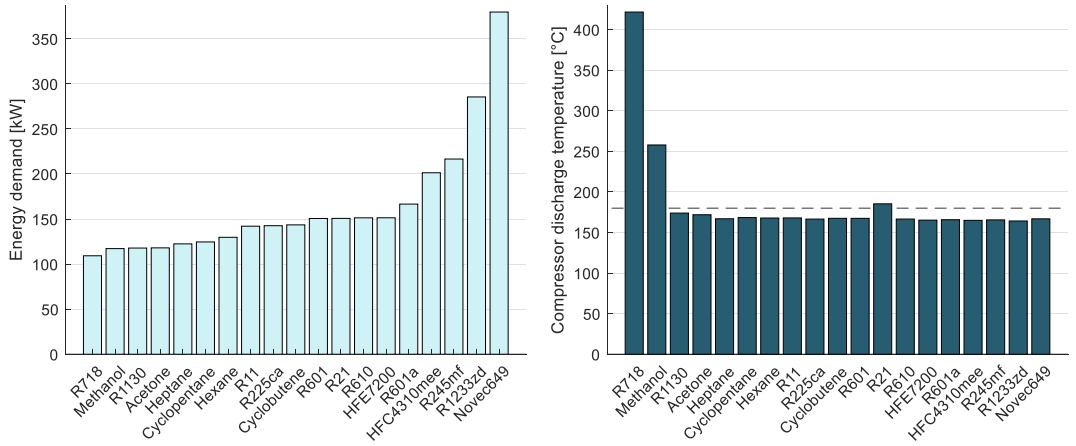

Fig. 13. Energy demand (left) of column with EHP and discharge temperatures (right) for thermodynamically feasible refrigerants for separation of hexanol-decanol.

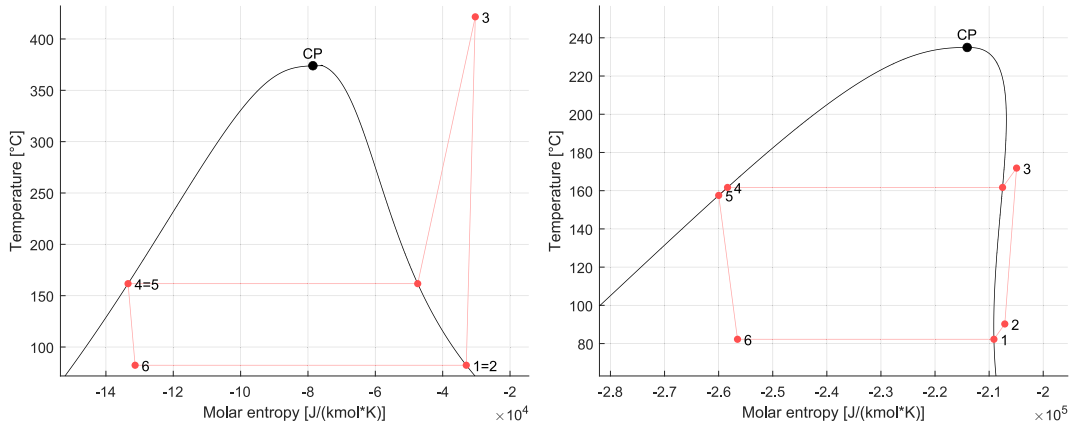

Fig. 14. T-s-diagrams of water (left) and acetone (right) with operating points of heat pump for separation of hexanol-decanol.

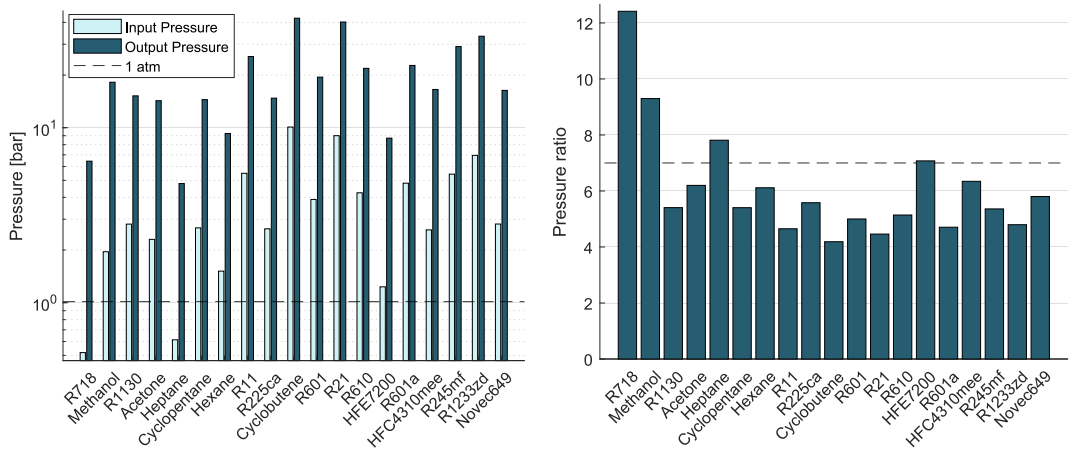

Fig. 15. Pressure levels (left) and pressure ratios (right) of heat pumps for thermodynamically feasible refrigerants for separation of hexanol-decanol.

4.2. Optimization of competing process designs

After successful identification of suitable refrigerants in the shortcut-based screening, the three refrigerants with the lowest net energy demand are selected and further analyzed in the techno-economic optimization of the heat pump-assisted distillation processes. The energetic and economic performance of the different EHP designs is compared with optimized designs of the conventional column and flash-enhanced VRC-assisted distillation. The product purities are constrained to ≥99 % for the rigorous optimization and an initial number of 100 stages is used for both the rectifying and stripping section. For the atmospheric separation of the close-boiling mixture, trays are employed as column internals, whereas the use of structured packings is considered for the wide-boiling mixture under vacuum conditions to ensure negligible pressure drop, aligning with the model assumptions. All optimizations are performed with GAMS 34.3.0 on an Intel Core i7–14700 CPU, solving the respective NLP problems with SNOPT. Despite the sequence of problems solved in the polylithic modeling and solution approach,

Table 4
Top five refrigerants in terms of energy demand for separation of hexanol-decanol.

Refrigerant	R1130	Acetone	Cyclopentane	Hexane	R11
Energy demand [kW]	117.8	118.0	124.6	129.7	142.0
$COP_{heating}$ [-]	3.51	3.50	3.32	3.19	2.92
Compression ratio [-]	5.41	6.20	5.40	6.12	4.65
Superheating duty [kW]	0	12.6	52.4	135.2	5.0
Logarithmic mean temperature difference in IHX [K]	–	73.3	60.0	44.2	78.0
Refrigerant flow rate [mol/s]	19.1	17.5	19.8	18.4	28.4

each design is optimized with a computational time of less than 4 min for both separation problems.

4.2.1. Optimization results for close boiling mixture ($\Delta T = 4.9$ K)

An overview of the key results of the TAC-optimized designs for all five process alternatives is presented in Table 5. The number of equilibrium stages of all heat pump designs ranges from 150 to 156 in comparison to 161 stages for the conventional column for the separation of the very narrow boiling mixture. Interestingly, the reflux ratios are somewhat larger for the heat pump-assisted distillation processes, allowing for some reduction in column height at a slightly larger column diameter than the conventional column.

The net energy demand ranges between 5.2 % higher (R1130 and acetone) than the shortcut results to 10 % higher (cyclopentane), which is expected due to the approximation in the RBM and the compromise between operating and investment cost in the TAC optimization. As calculated during the screening, all EHP designs do not use external heat and are thus fully electrified. The VRC-assisted column with IHX and recycle stream also achieves full electrification with about half the compressor duty and external cooling demand of the EHP designs since the compression ratio for VRC is as expected lower than for the EHP designs, which are basically identical to the values from the shortcut screening. Overall, the results from the shortcut screening agree very well with the optimization results, such that the respective refrigerant screening can be effectively performed on the basis of the shortcut screening.

Fig. 16 and Fig. 17 present a breakdown of the different contributions to the energy demand and TAC for all optimized process configurations. The best performing EHP design using R1130 can reduce the net energy demand of the conventional column by 91.1 % while the flash-enhanced VRC enables 95.5 % savings. The extra energy requirement of the EHP stems from the minimum approach temperature of 10 K in the integrated heat exchangers that needs to be compensated twice for the EHP designs, requiring a higher compressor duty. This is particularly important for the separation of such a close boiling mixture, for which the impact of the additional approach temperature is particularly large, as the temperature difference of 24.9 K for EHP is 67.1 % larger than the 14.9 K for VRC in this case.

The energy savings of the flash-enhanced VRC translate into a TAC reduction of 65.7 % compared to the conventional column. As for the energy requirements, the EHP designs are providing lower economic benefits than VRC both regarding capital costs and operating costs. Therefore, the relative performance deficit would not be compensated for different depreciation times. The higher operating costs for EHP are a direct consequence of the higher net energy requirement, which also results in a larger and thus more expensive compressor. The additional heat exchanger area for the increased heat transfer further increases the capital cost compared to the VRC design, but all designs still yield ~50 % lower TAC compared to the conventional process. The IHX for VRC and EHP with cyclopentane are comparatively small and accordingly do not influence the costs significantly.

4.2.2. Optimization results for wide boiling mixture ($\Delta T = 59.4$ K)

The design parameters and performance metrics of the techno-economically optimized processes for the separation of the wide boiling mixture are summarized in Table 6. Notably, each optimization results in a column design with just 8 or 9 stages (less than 5 % of stages in superstructure) and a column diameter of 0.96 m, highlighting the effective optimization of the column design. A major beneficial factor of the EHP designs is the respective compression ratio, which is still below the threshold value of 7 for single stage compression, whereas the VRC-assisted design exceeds this value with 13.8 almost by a factor of 2. This illustrates an important operational benefit of EHP over VRC, making them particularly interesting for wider boiling systems.

It is also important to note that as the distillation column operates at 0.08 bar, the open cycle compression for VRC would require operation under vacuum conditions, which would generally require a larger compressor and piping. The subsequent economic assessment of the VRC-assisted design serves therefore rather as an idealistic reference, since these factors are not appropriately reflected in the applied cost correlations, and it is expected that the true costs for the VRC-assisted design would be considerably higher than the presented values. The EHP designs are not affected, as all compression cycles operate above atmospheric pressure with reasonable compression ratios. Therefore, while VRC demonstrates superior performance compared to all EHP designs in terms of both energy and costs discussed in more detail in the following, its practical implementation proves challenging in this case.

While the separation of such a wide boiling mixture is considerably easier compared to the close boiling mixture, as evident from the much lower number of stages and net energy demand of the conventional column of 397 kW, the efficiency of the heat pump designs diminishes due to the larger temperature lift, leading to smaller relative energy savings.

For the wide-boiling mixture, the EHP's additional approach temperature contributes only 14.9 % to the total temperature lift compared

Table 5
Key results of TAC-optimal designs for different process alternatives for separation of equimolar benzene-fluorobenzene mixture.

Process	Conventional column	Flash-enhanced VRC	EHP: R1130	EHP: Acetone	EHP: Cyclopentane
Reboiler duty (kW)	2940	0	0	0	0
Condenser duty (kW)	−2929	0	−255	−260	−297
Additional condenser duty (kW)	–	−129	–	–	–
IHX duty (kW)	–	8.5	0	0	54.4
Compression ratio	–	1.550	1.920	2.045	1.930
Compressor duty (kW)	–	133	259	264	283
Reflux ratio	18.09	18.34	18.36	18.20	18.36
Number of stages in rectif./strip. section	107/54	105/46	107/43	106/50	107/43
Diameter (m)	1.776	1.787	1.788	1.781	1.788
Annual operating cost (k€/a)	1218.8	68.7	133.5	136.1	146.3
Annual capital cost (k€/a)	318.8	458.7	622.4	630.4	638.4
Total annual cost (k€/a)	1537.7	527.5	755.9	766.5	784.7
Computation time (s)	100	69	88	60	69

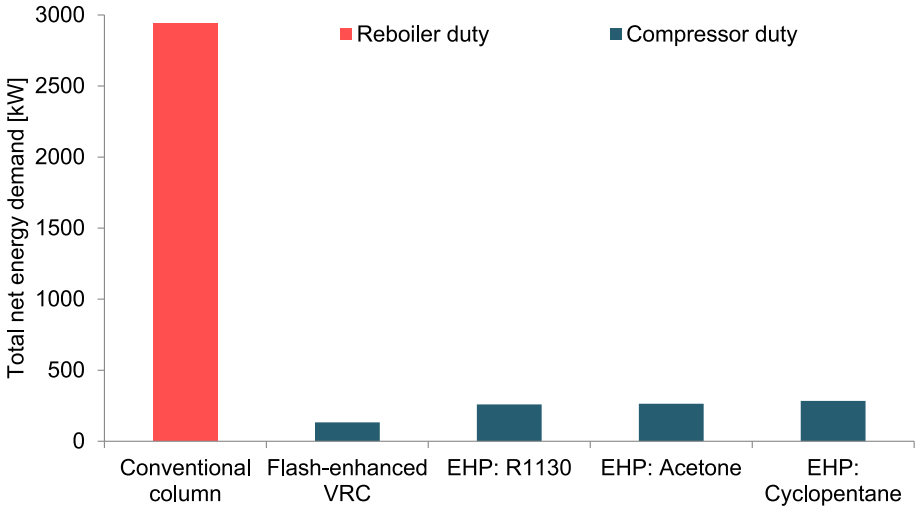

Fig. 16. Total net energy demand of TAC-optimal designs for different process alternatives for separation of equimolar benzene-fluorobenzene mixture.

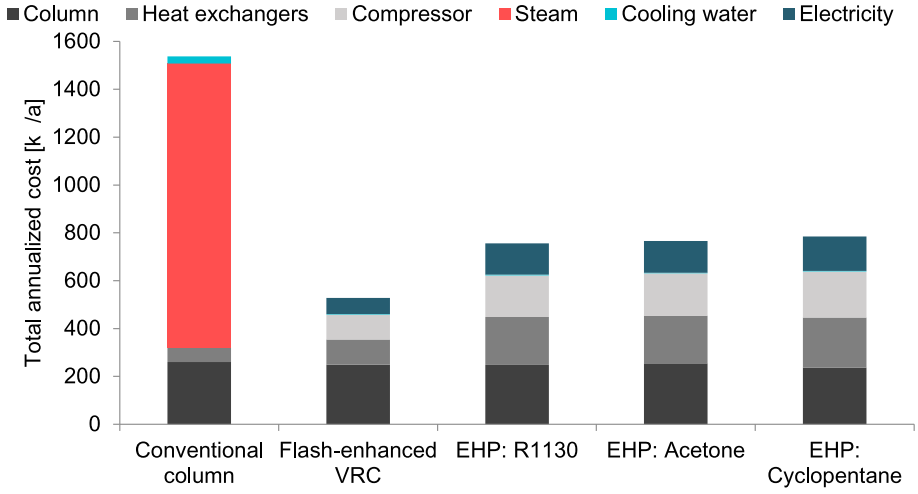

Fig. 17. TAC breakdown of TAC-optimal designs for different process alternatives for separation of equimolar benzene-fluorobenzene mixture.

Table 6
Key results of TAC-optimal designs for different process alternatives for separation of equimolar hexanol-decanol mixture.

Process	Conventional column	Flash-enhanced VRC	EHP: R1130	EHP: Acetone	EHP: Cyclopentane
Reboiler duty (kW)	397	0	0	0	0
Condenser duty (kW)	−318	0	−30.3	−34.1	−51.9
Additional condenser duty (kW)	–	−5.7	–	–	–
IHX duty (kW)	–	38.5	0	9.3	42.6
Compression ratio	–	13.827	5.385	6.175	5.384
Compressor duty (kW)	–	84.2	108.8	112.6	130.4
Reflux ratio	0.146	0.152	0.152	0.146	0.146
Number of stages in rectif./strip. section	4/5	3/5	3/5	4/5	4/5
Diameter (m)	0.958	0.960	0.960	0.958	0.958
Annual operating cost (k€/a)	162.1	42.9	55.3	57.2	66.4
Annual capital cost (k€/a)	50.1	117.2	149.1	152.3	164.0
Total annual cost (k€/a)	212.3	160.2	204.4	209.6	230.4
Computation time (s)	149	188	63	61	57

to the VRC design. Despite this, all three EHP designs exhibit higher net energy demand than the VRC, with the best EHP design with R1130 requiring 29.2 % more energy than the VRC design. Still, the best EHP design saves 71.3 % net energy over the conventional process while the flash-enhanced VRC design delivers 77.8 % net energy savings. As for the separation of the close-boiling mixture, all heat pump designs are fully electrified since both VRC and EHP models allow for the flow rate though the compression cycle to be adjusted, perfectly matching the integrated amount of heat to the heat demand of the column. Fig. 18 and Fig. 19 provide the net energy and cost breakdown for the individual process designs.

Due to the large capital investment for the compressor and additional

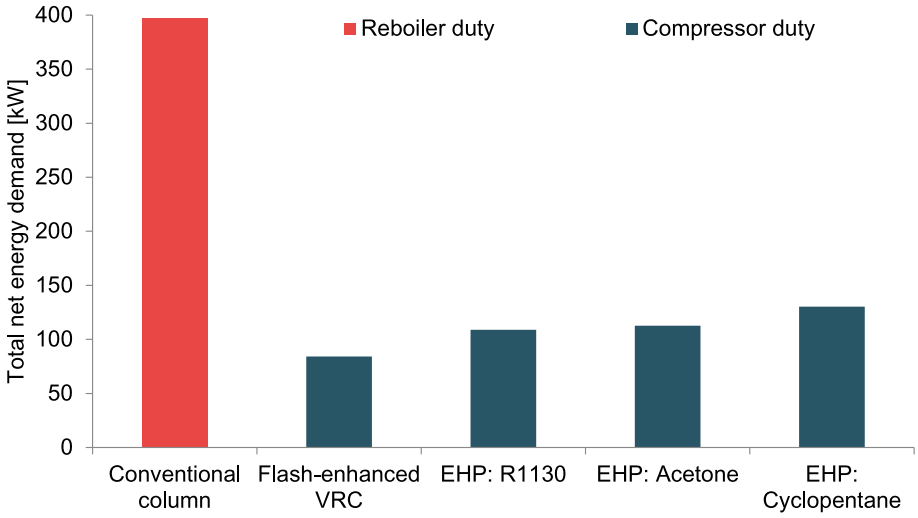

Fig. 18. Total energy demand of TAC-optimal designs for different process alternatives for separation of equimolar hexanol-decanol mixture.

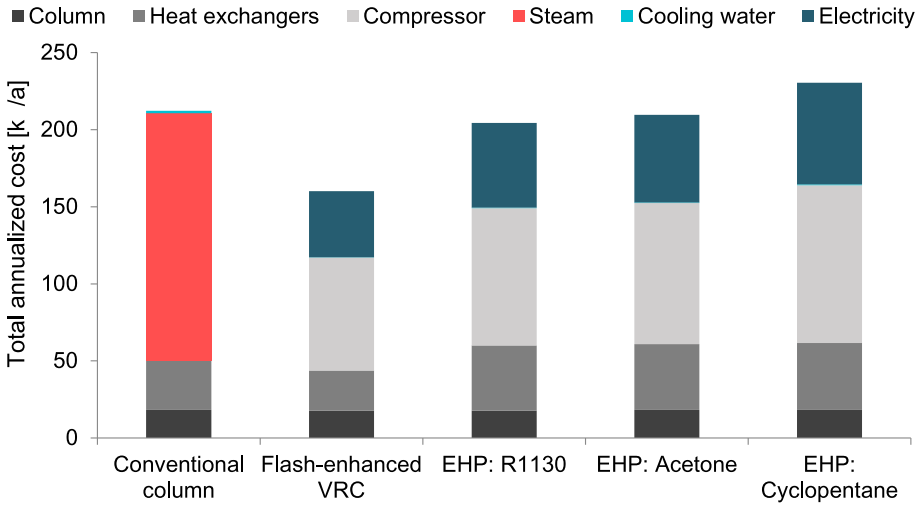

Fig. 19. TAC breakdown of TAC-optimal designs for different process alternatives for separation of equimolar hexanol-decanol mixture.

heat exchanger in the case of EHP, the capital costs for VRC is more than twice the capital cost of the conventional process and the cheapest EHP design is three times as expensive. However, the heat pump processes yield significantly lower operating costs than a conventional process (73.5 % lower for VRC, 65.8 % lower for best EHP design), which means these types of processes perform better when longer depreciation periods are considered. Considering the given depreciation, the best two EHP designs with R1130 and acetone still provide a small TAC advantage of 3.7 % and 1.3 % over a conventional process which grow to 15.9 % and 13.7 % when the depreciation time is extended to 15 years for the given process designs.

5. Conclusion

This current study presents a two-step method for the design and evaluation of heat pump-assisted distillation processes to efficiently calculate heat pump cycles for pure subcritical refrigerants tailored to the heat sink and heat source temperature levels and duties of the respective separation problem. The current implementation of the method performs an efficient shortcut-based evaluation of 39 potential refrigerants from ten different molecule groups based on the minimum heat duties for a specific separation problem calculated with the Rectification Body Method, evaluating the necessary heat pump design, performance metrics, as well as thermodynamic and practical constraints, requiring just seconds of computational time. The most promising refrigerants are subsequently evaluated in a techno-economic optimization against conventional and flash-enhanced VRC processes.

The results of the computational study for two exemplary separation problems, including a close-boiling benzene-fluorobenzene and a wide-boiling hexanol-decanol separation, illustrate that EHPs can enable substantial energy savings even for larger temperature lifts of 77 K with different refrigerants. For both separations studied, the same five refrigerants R1130, acetone, cyclopentane, hexane and R11 are the energetically most attractive after accounting for practical limitations.

For both the close and wide boiling mixture, all heat pump processes provide significantly lower net energy demands than a conventional process and enable fully electrified distillation. Thus, an operation with a substantially reduced amount of renewable energy becomes feasible. This effectively contributes to SDG 7 (Affordable and Clean Energy) by improving energy efficiency, SDG 9 (Industry, Innovation, and Infrastructure) by supporting the decarbonization of industrial processes, SDG 12 (Responsible Consumption and Production) by promoting resource efficiency, and SDG 13 (Climate Action) by reducing CO_2 emissions in energy-intensive sectors.

For the close boiling mixture separated with distillation under vacuum conditions, the energy savings of all three closed cycle designs

provide translates into lower total annualized costs than a conventional column and even for the wide-boiling mixture, modest cost savings are attainable with the best-performing closed-cycle design. Where practical constraints permit, flash-enhanced VRC outperforms closed-cycle heat pumps energetically and economically due to the large impact of the additional approach temperature necessary for the latter. Nonetheless, closed-cycle offer compelling retrofit opportunities and can overcome operational challenges when VRC is not applicable, such as with thermally sensitive product streams or high compression ratios. This advantage is demonstrated with the wide-boiling mixture, where closed cycle designs require much lower compression ratios and allow operation of the heat pump at above-atmospheric conditions.

Future extensions of heat pump-assisted design should incorporate detailed pressure drop calculations. For vacuum distillation, as investigated by Rix *et al.* [17], and for very narrow boiling systems such as the benzene-fluorobenzene system considered in this work, the cumulative pressure drop can significantly affect the bottom stream temperature and, consequently, the required temperature lift. Since an increased bottom temperature influences the suitability and performance of the refrigerants, accounting for this prior to refrigerant screening by calculating the bottom temperature with the pressure drop in mind will be valuable. Furthermore, integrating pressure drop estimations directly into the optimization model would enhance the accuracy of energy demand predictions and lead to more robust process designs.

The presented shortcut screening approach for refrigerant selection and heat pump design has a broad applicability beyond distillation processes, as it only requires knowledge of the heat source and heat sink. Future work may therefore explore different applications including the use for plant-wide heat integration [74,75]. Additionally, it can be extended to optimize refrigerant mixtures for specific applications, considering temperature glides and compensating for unfavorable refrigerant properties. Zeotropic mixtures have different dew point and bubble point temperatures. The resulting temperature glide is beneficial for process media with large temperature glides in the heat sink and source, as the exergy loss due to heat transfer can be reduced by matching the temperature profile to the external fluid [41,46,47]. The temperature lift of the cycle can be reduced, leading to improved cycle efficiency [41]. In that context, the models may be improved in different directions, developing tailored external equations or extrinsic functions for enthalpy and entropy computations, improved cost correlations for compressor costs, as well as extending the process models to consider intermediate heat exchangers, as these can effectively reduce the internal exergy losses in distillation columns [35].

CRediT authorship contribution statement

Momme Adami: Conceptualization, Software, Investigation, Writing – original draft, Writing – review & editing, Project administration, Visualization. **Jonas Schnurr:** Methodology, Software, Validation, Investigation, Writing – original draft, Visualization. **Mirko Skiborowski:** Resources, Supervision, Writing – review & editing.

Declaration of generative AI and AI-assisted technologies in the writing process

During the preparation of this work the authors used ChatGPT in order to aid in formulation of text sections. After using this tool/service, the authors reviewed and edited the content as needed and take full responsibility for the content of the publication.

Declaration of competing interest

The authors declare that they have no known competing financial interests or personal relationships that could have appeared to influence the work reported in this paper.

Acknowledgements

This research did not receive any specific grant from funding agencies in the public, commercial, or not-for-profit sectors.

Appendix A. Supplementary material

Supplementary data to this article can be found online at https://doi.org/10.1016/j.applthermaleng.2025.126559.

Data availability

Data will be made available on request.

References

[1] M. Ahmed, Ed., *Global Agricultural Production Resilience to Climate Change*, 1st ed. Cham: Springer International Publishing; Imprint: Springer, 2022. Accessed: Nov. 30 2023. [Online]. Available: #page=8.
[2] F. Schlosser, M. Jesper, J. Vogelsang, T.G. Walmsley, C. Arpagaus, J. Hesselbach, Large-scale heat pumps: applications, performance, economic feasibility and industrial integration, *Renew. Sustain. Energy Rev.* 133 (2020) 110219, https://doi.org/10.1016/j.rser.2020.110219.
[3] R.T. Gooty, R. Agrawal, M. Tawarmalani, Advances in MINLP to identify energy-efficient distillation configurations, *Oper. Res.* 72 (2) (2024) 639–659, https://doi.org/10.1287/opre.2022.2340.
[4] Oak Ridge National Laboratory, Materials for Separation Technologies. Energy and Emission Reduction Opportunities, 2005.
[5] A.A. Kiss, R. Smith, Rethinking energy use in distillation processes for a more sustainable chemical industry, *Energy* 203 (2020) 1–12, https://doi.org/10.1016/j.energy.2020.117788.
[6] J.A. Chavez Velasco, M. Tawarmalani, R. Agrawal, Systematic analysis reveals thermal separations are not necessarily most energy intensive, *Joule* 5 (2) (2021) 330–343, https://doi.org/10.1016/j.joule.2020.12.002.
[7] R. Agrawal, R.T. Gooty, Misconceptions about efficiency and maturity of distillation, *AIChE J.* 66 (8) (2020), https://doi.org/10.1002/aic.16294.
[8] R.T. Gooty, J.A.C. Velasco, R. Agrawal, Methods to assess numerous distillation schemes for binary mixtures, *Chem. Eng. Res. Des.* 172 (2021) 1–20, https://doi.org/10.1016/j.cherd.2021.05.022.
[9] M. Skiborowski, K.F. Kruber, T. Waltermann, Sustainable Distillation Processes, Wiley, 2022, pp. 431–481.
[10] J.A. Chavez Velasco, M. Tawarmalani, R. Agrawal, Which separation scenarios are advantageous for membranes or distillations? *AIChE J.* 68 (11) (2022) https://doi.org/10.1002/aic.17839.
[11] Y. Dong, H. Madani, X. Kou, R. Wang, High temperature heat pump with dual uses of cooling and heating for industrial applications, *Appl. Energy* 379 (2025) 124962, https://doi.org/10.1016/j.apenergy.2024.124962.
[12] A.A. Kiss, C.A.I. Ferreira, *Heat pumps in chemical process industry*, CRC Press Taylor & Francis Group, Boca Raton, London, New York, 2017.
[13] L. Xu, M. Li, X. Yin, X. Yuan, New intensified heat integration of vapor recompression assisted dividing wall column, *Ind. Eng. Chem. Res.*, 56 (8) (2017) 2188–2196, https://doi.org/10.1021/acs.iecr.6b03802.
[14] C. Cui, et al., Electrification of distillation for decarbonization: an overview and perspective, *Renew. Sustain. Energy Rev.* 199 (2024) 114522, https://doi.org/10.1016/j.rser.2024.114522.
[15] A. Marina, S. Spoelstra, H.A. Zondag, A.K. Wemmers, An estimation of the European industrial heat pump market potential, *Renew. Sustain. Energy Rev.* 139 (2021) 110545, https://doi.org/10.1016/j.rser.2020.110545.
[16] C. Arpagaus, F. Bless, M. Uhlmann, J. Schiffmann, S.S. Bertsch, High temperature heat pumps: market overview, state of the art, research status, refrigerants, and application potentials, *Energy* 152 (2018) 985–1010, https://doi.org/10.1016/j.energy.2018.03.166.
[17] A. Rix, M. Schröder, N. Paul, Vapor recompression: an interesting option for vacuum columns? *Chem. Eng. Res. Des.* 191 (2023) 226–235, https://doi.org/10.1016/j.cherd.2023.01.030.
[18] D.R. Woods, *Rules of Thumb in Engineering Practice*, Wiley, 2007.
[19] R. Smith, *Chemical Process Design and Integration*, John Wiley & Sons, Ltd, 2005.
[20] T. Fan, B. Wang, C. Yan, W. Zhang, Z. Song, X. Zheng, Effect of self-recirculating casing treatment on the aerodynamic performance of ultra-high-pressure-ratio centrifugal compressors, *Processes* 11 (8) (2023) 2439, https://doi.org/10.3390/pr11082439.
[21] Y. Zhang, Z. Zhang, X. Dong, G. Han, Y. Zhang, X. Lu, Effects of unsteady interaction on the performance of an ultra-high-pressure-ratio centrifugal compressor, *Aerosp. Sci. Technol.* 105 (2020) 106036, https://doi.org/10.1016/j.ast.2020.106036.
[22] M. Vagani, C.D. Bolin, Design and Performance Evaluation of a 10:1 Pressure Ratio Centrifugal Compressor Impeller. *Proceedings of the ASME 2010 International Mechanical Engineering Congress & Exposition*, 2010.
[23] A.A. Kiss, S.J. Flores Landaeta, C.A. Infante Ferreira, Towards energy efficient distillation technologies – making the right choice, *Energy* 47 (1) (2012) 531–542, https://doi.org/10.1016/j.energy.2012.09.038.

[24] S.D. Barnicki, J.R. Fair, Separation system synthesis: a knowledge-based approach. 1. liquid mixture separations, *Ind. Eng. Chem. Res.*, 29 (3) (1990) 421–432, https://doi.org/10.1021/ie00099a018.

[25] C.A. Jaksland, R. Gani, K.M. Lien, Separation process design and synthesis based on thermodynamic insights, *Chem. Eng. Sci.* 50 (3) (1995) 511–530, https://doi.org/10.1016/0009-2509(94)00216-E.

[26] A. Kazemi, A. Mehrabani-Zeinabad, M. Beheshti, Recently developed heat pump assisted distillation configurations: a comparative study, *Appl. Energy* 211 (2018) 1261–1281, https://doi.org/10.1016/j.apenergy.2017.12.023.

[27] A. Kazemi, A. Mehrabani-Zeinabad, M. Beheshti, Distillation without hot utilities; development of novel distillation configurations for energy and costs saving for separation of propylene/propane mixture, *Chem. Eng. Process. - Process Intesif.* 123 (2018) 158–167, https://doi.org/10.1016/j.cep.2017.10.027.

[28] S. Supranto, Heat pump assisted distillation.: I: alternative ways to minimize energy consumption in fractional, *Energy Research* 10 (1986) 145–161.

[29] A.K. Jana, Advances in heat pump assisted distillation column: a review, *Energ. Conver. Manage.* 77 (2014) 287–297, https://doi.org/10.1016/j.enconman.2013.09.055.

[30] A.K. Jana, Heat integrated distillation operation, *Appl. Energy* 87 (5) (2010) 1477–1494, https://doi.org/10.1016/j.apenergy.2009.10.014.

[31] A.A. Shenvi, D.M. Herron, R. Agrawal, Energy efficiency limitations of the conventional heat integrated distillation column (HIDiC) configuration for binary distillation, *Ind. Eng. Chem. Res.* 50 (1) (2011) 119–130, https://doi.org/10.1021/ie101698f.

[32] A. Harwardt, W. Marquardt, Heat-integrated distillation columns: Vapor recompression or internal heat integration? *AIChE J.* 58 (12) (2012) 3740–3750, https://doi.org/10.1002/aic.13775.

[33] M. Adami, K. Farheen, M. Skiborowski, Electrifying distillation – Optimization-based evaluation of internally heat-integrated distillation columns, *Sep. Purif. Technol.* (2024) 131061, https://doi.org/10.1016/j.seppur.2024.131061.

[34] X. You, I. Rodriguez-Donis, V. Gerbaud, Reducing process cost and CO2 emissions for extractive distillation by double-effect heat integration and mechanical heat pump, *Appl. Energy* 166 (2016) 128–140, https://doi.org/10.1016/j.apenergy.2016.01.028.

[35] M. Skiborowski, K.F. Kruber, "Exergy-based optimization for the synthesis of heat pump assisted distillation columns," in *Computer Aided Chemical Engineering*, Elsevier, 2024, pp. 1351–1356.

[36] G. Modla and P. Lang, "Decrease of the energy demand of distillation with vapour recompression," *Proceedings of the 5th international scientific conference on advances in mechanical engineering (ISCAME 2017) Debrecen, Hungary*, 2017.

[37] L. Hegely, P. Lang, Optimisation of the higher pressure of pressure-swing distillation of a maximum azeotropic mixture, *Energy* 271 (2023) 126939, https://doi.org/10.1016/j.energy.2023.126939.

[38] M. Ferchichi, L. Hegely, P. Lang, Economic and environmental evaluation of heat pump-assisted pressure-swing distillation of maximum-boiling azeotropic mixture water-ethylenediamine, *Energy* 239 (2022) 122608, https://doi.org/10.1016/j.energy.2021.122608.

[39] C. Cui, X. Zhang, M. Qi, H. Lyu, J. Sun, A.A. Kiss, Fully electrified heat pump assisted distillation process by flash vapour circulation, *Chem. Eng. Res. Des.* 206 (2024) 280–284, https://doi.org/10.1016/j.cherd.2024.05.011.

[40] A.S. Nogaja, M. Tawarmalani, R. Agrawal, Cogeneration improves separation efficiency, *Ind. Eng. Chem. Res.*, 63 (43) (2024) 18564–18574, https://doi.org/10.1021/acs.iecr.4c03190.

[41] A. Fernández-Moreno, A. Mota-Babiloni, P. Giménez-Prades, J. Navarro-Esbrí, Optimal refrigerant mixture in single-stage high-temperature heat pumps based on a multiparameter evaluation, *Sustainable Energy Technol. Assess.* 52 (2022) 101989, https://doi.org/10.1016/j.seta.2022.101989.

[42] W. Grassi, *Heat Pumps: Fundamentals and Applications*, Springer, Cham, 2018.

[43] *Kälteanlagen und Wärmepumpen – Sicherheitstechnische und umweltrelevante Anforderungen – Teil 1: Grundlegende Anforderungen, Begriffe, Klassifikationen und Auswahlkriterien; Deutsche Fassung EN 378-1:2016+A1:2020*, 378-1, Europäisches Komitee für Normung, 2020.

[44] *ANSI/ASHRAE Addendum f to ANSI/ASHRAE Standard 34-2019,* ASHRAE, 2019.

[45] B.S. Oh, J. Cho, B. Choi, H.W. Choi, M.S. Kim, G. Lee, Application of heuristic algorithms for design optimization of industrial heat pump, *Int. J. Refrig.* 134 (2022) 1–15, https://doi.org/10.1016/j.ijrefrig.2021.11.002.

[46] L. Zhang, J. Zhao, L. Yue, H. Zhou, C. Ren, Cycle performance evaluation of various R134a/hydrocarbon blend refrigerants applied in vapor-compression heat pumps, *Adv. Mech. Eng.* 11 (1) (2019) 168781401881956, https://doi.org/10.1177/1687814018819561.

[47] B. Zühlsdorf, J.K. Jensen, S. Cignitti, C. Madsen, B. Elmegaard, Analysis of temperature glide matching of heat pumps with zeotropic working fluid mixtures for different temperature glides, *Energy* 153 (2018) 650–660, https://doi.org/10.1016/j.energy.2018.04.048.

[48] W.-T. Tsai, Environmental risk assessment of hydrofluoroethers (HFEs), *J. Hazard. Mater.* 119 (1–3) (2005) 69–78, https://doi.org/10.1016/j.jhazmat.2004.12.018.

[49] S. Supranto, Heat pump assisted distillation.: II: matching an external heat pump to a fractional distillation system, *Energy Res.* 10 (1986) 235–254.

[50] S.B.M. Oliveira, J.A.R. Parise, R.P. Marques, Modelling of an ethanol-water distillation column assisted by an external heat pump, *Int. J. Energy Res.* 26 (12) (2002) 1055–1072, https://doi.org/10.1002/er.834.

[51] C.C.S. Reddy, Y. Fang, G.P. Rangaiah, Improving energy efficiency of distillation using heat pump assisted columns, *Asia-Pacific J. Chem. Eng.* 9 (6) (2014) 905–928, https://doi.org/10.1002/apj.1842.

[52] C. Mateu-Royo, C. Arpagaus, A. Mota-Babiloni, J. Navarro-Esbrí, S.S. Bertsch, Advanced high temperature heat pump configurations using low GWP refrigerants for industrial waste heat recovery: a comprehensive study, *Energ. Conver. Manage.* 229 (2021) 113752, https://doi.org/10.1016/j.enconman.2020.113752.

[53] S. Koundinya, S. Seshadri, Energy, exergy, environmental, and economic (4E) analysis and selection of best refrigerant using TOPSIS method for industrial heat pumps, *Therm. Sci. Eng. Prog.* 36 (2022) 101491, https://doi.org/10.1016/j.tsep.2022.101491.

[54] J. Jiang, B. Hu, T. Ge, R.Z. Wang, Comprehensive selection and assessment methodology of compression heat pump system, *Energy* 241 (2022) 122831, https://doi.org/10.1016/j.energy.2021.122831.

[55] M.P. Andersen, B. Zühlsdorf, W.B. Markussen, J.K. Jensen, B. Elmegaard, Selection of working fluids and heat pump cycles at high temperatures: Creating a concise technology portfolio, *Appl. Energy* 376 (2024) 124312, https://doi.org/10.1016/j.apenergy.2024.124312.

[56] J. Mairhofer, M. Stavrou, A multi-criteria study of optimal working fluids for high temperature heat pumps, *Chem. Ing. Tech.* 95 (3) (2023) 458–466, https://doi.org/10.1002/cite.202200106.

[57] J. S. Daniel, G. Velders, A. R. Douglass, and P. Forster, "Halocarbon Scenarios, Ozone Depletion Potentials, and Global Warming Potentials," *NOAA Chemical Sciences Laboratory*, 2007.

[58] 3M Electronics Materials Division, Ed., *Product Information 3M Novec 7200*, 2009.

[59] P. Giménez-Prades, J. Navarro-Esbrí, C. Arpagaus, A. Fernández-Moreno, A. Mota-Babiloni, Novel molecules as working fluids for refrigeration, heat pump and organic Rankine cycle systems, *Renew. Sustain. Energy Rev.* 167 (2022) 112549, https://doi.org/10.1016/j.rser.2022.112549.

[60] P. Office, *Regulation (EU) No 517/2014 of the European Parliament and of the Council of 16 April 2014 on fluorinated greenhouse gases and repealing Regulation (EC) No 842/2006Text with EEA relevance*, 2014.

[61] C. Höges, V. Venzik, C. Vering, and D. Müller, "Decarbonizing Steam Generation with High Temperature Heat Pumps: Refrigerant Selection and Flowsheet Evaluation," Lehrstuhl für Gebäude- und Raumklimatechnik RWTH-2023-05615, 2023. [Online]. Available: https://publications.rwth-aachen.de/record/959445.

[62] E. P. SNAP, Ed., *TRANSITIONING TO LOW-GWP ALTERNATIVES in Aerosols*, 2016.

[63] B. Gil, J. Kasperski, Efficiency analysis of alternative refrigerants for ejector cooling cycles, *Energ. Conver. Manage.* 94 (2015) 12–18, https://doi.org/10.1016/j.enconman.2015.01.056.

[64] 3M Deutschland, *Datenblatt 3M Novec 649 High-Tech Flüssigkeit*.

[65] J. Bausa, R. von Watzdorf, W. Marquardt, Shortcut methods for nonideal multicomponent distillation: I. Simple columns, *AIChE J.* 44 (10) (1998) 2181–2198, https://doi.org/10.1002/aic.690441008.

[66] M. Skiborowski, A. Harwardt, W. Marquardt, Conceptual design of azeotropic distillation processes, in: *Distillation*, Elsevier, 2014, pp. 305–355.

[67] K. Kraemer, S. Kossack, W. Marquardt, Efficient optimization-based design of distillation processes for homogeneous azeotropic mixtures, *Ind. Eng. Chem. Res.*, 48 (14) (2009) 6749–6764, https://doi.org/10.1021/ie900143e.

[68] M. Skiborowski, A. Harwardt, W. Marquardt, Efficient optimization-based design for the separation of heterogeneous azeotropic mixtures, *Comput. Chem. Eng.* 72 (5) (2015) 34–51, https://doi.org/10.1016/j.compchemeng.2014.03.012.

[69] T. Waltermann, M. Skiborowski, Efficient optimization-based design of energy-integrated distillation processes, *Comput. Chem. Eng.* 129 (8) (2019) 106520, https://doi.org/10.1016/j.compchemeng.2019.106520.

[70] L.T. Biegler, *Systematic methods of chemical process design*, Prentice Hall PTR, Upper Saddle River, N.J., 1997.

[71] R. Turton, *Analysis, synthesis, and design of chemical processes,* 3rd ed. Upper Saddle River, N.J., Boston, Mass.: Prentice Hall; Safari Books Online, 2009. [Online]. Available: https://learning.oreilly.com/library/view/-/9780135072912/?ar.

[72] T. Waltermann, S. Sibbing, M. Skiborowski, Optimization-based design of dividing wall columns with extended and multiple dividing walls for three- and four-product separations, *Chem. Eng. Process. - Process Intesif.* 146 (2019) 107688, https://doi.org/10.1016/j.cep.2019.107688.

[73] W.L. Luyben, Compressor heuristics for conceptual process design, *Ind. Eng. Chem. Res.*, 50 (24) (2011) 13984–13989, https://doi.org/10.1021/ie202027h.

[74] B. de Raad, M. van Lieshout, L. Stougie, A. Ramirez, Improving plant-level heat pump performance through process modifications, *Appl. Energy* 358 (2024) 122667, https://doi.org/10.1016/j.apenergy.2024.122667.

[75] M. Yang, X. Feng, G. Liu, Heat integration of heat pump assisted distillation into the overall process, *Appl. Energy* 162 (2016) 1–10, https://doi.org/10.1016/j.apenergy.2015.10.044.